Chemical Engineering Journal 473 (2023) 145297

Contents lists available at ScienceDirect

Chemical Engineering Journal

journal homepage: www.elsevier.com/locate/cej

Flexible thermoelectric energy harvesting system based on polymer composites

T. Rodrigues-Marinho [a,b], V. Correia [c,d], C.-R. Tubio [f], A. Ares-Pernas [e], M.-J. Abad [e], S. Lanceros-Méndez [a,b,f,g,*], P. Costa [a,b,h,*]

[a] Physics Centre of Minho and Porto Universities (CF-UM-UP), University of Minho, 4710-057, Portugal
[b] LaPMET – Laboratory of Physics for Materials and Emergent Technologies, University of Minho, 4710-057, Portugal
[c] Center for MicroElectromechanical Systems (CMEMS), University of Minho, Campus de Azurém, 4800-058 Guimarães, Portugal
[d] LABBELS – Associate Laboratory in Biotechnology and Bioengineering and Microelectromechanical Systems, Universidade do Minho, Braga/Guimarães, Portugal
[e] Universidade da Coruña, Campus Industrial de Ferrol, CITENI, Grupo de Polímeros, Campus de Esteiro, 15403 Ferrol, Spain
[f] BCMaterials, Basque Center for Materials, Applications and Nanostructures, UPV/EHU Science Park, 48940 Leioa, Spain
[g] IKERBASQUE, Basque Foundation for Science, 48009 Bilbao, Spain
[h] Institute for Polymers and Composites, IPC, University of Minho, 4800-058, Guimarães, Portugal

ARTICLE INFO

Keywords:
Energy harvesting
Polymers matrices
Ceramic
Printing materials
Easy processing

ABSTRACT

Flexible and easy processing lightweight thermoelectric materials for energy harvesting applications have shown an increasing interest. Thermoplastic polyvinylidene fluoride (PVDF) and elastomer styrene-ethylene/butylene-styrene (SEBS) polymers reinforced with thermoelectric ceramics, including bismuth sulfide (Bi_2S_3), bismuth telluride (Bi_2Te_3) and antimony telluride (Sb_2Te_3), and electrically conductive carbon nanotubes (CNT) have been developed, tailoring their thermal and electrical properties for thermoelectric device applications. The Seebeck coefficient of the composites increases with thermoelectric ceramic filler content for semicrystalline PVDF composites, slightly decreasing for amorphous SEBS composite. Thermoelectric power factor and figure-of-merit in the polymer composites increases up to 9 orders of magnitude with respect to the pristine polymer, up to a maximum value of 10^{-3} μW/(m·K^2) and 10^{-6}, respectively, for the PVDF/CNT/Bi_2Te_3 composite. A device composed by 2 printable p-n thermocouples based on PVDF/50Bi_2S_3 and PVDF/50Bi_2Te_3 can generate power in the order of the nW and charge a capacitor with 5 V. Theoretical modeling allows to evaluate different thermoelectric configurations, the effect of the number of thermocouples and the influence of the temperature gradient on device performance.

1. Introduction

The social and economic paradigms are rapidly changing with an enormous increase in the use and areas of application of low-power and wearable devices used in daily activities worldwide, in the scope of the Internet of Things and Industry 4.0 paradigms [1]. Energy is an essential indicator of social and economic progress, and the annual global demand for energy consumption has risen exponentially in the last few decades and will continue to increase; predicted to increase by near 50% for the next 3 decades [2,3]. Nevertheless, it is mandatory to reduce energy waste and several strategies are being implemented to increase energy transformation and consumption efficiency [4], since it is estimated that about half of the global primary energy production is dissipated by heat [5]. Thus, thermoelectric (TE) energy harvesting systems can be used to take advantage of the thermal energy dissipated as heat, in order to produce electrical energy for low-power devices [6]. Further, the growth of portable electronic devices and wearable sensors [7] demands sustainable green energy sources [8] and energy harvesting of low-power devices [9] is expected to have high growth in the next few years. In particular, the TE effect can be a promising strategy to recover a portion of wasted heat energy, either from the human body or environment (solar, as an example), or from industrial processes, since it is based on the conversion of a temperature gradient into an electrical voltage (Seebeck effect) or viceversa (Peltier effect) [10]. The performance evaluation of a TE device is commonly evaluated using the dimensionless figure-of-merit (ZT) and power factor (PF) [11,12].

* Corresponding authors at: Physics Centre of Minho and Porto Universities (CF-UM-UP), University of Minho, 4710-057, Portugal.
E-mail addresses: senentxu.lanceros@bcmaterials.net (S. Lanceros-Méndez), pcosta@fisica.uminho.pt (P. Costa).

https://doi.org/10.1016/j.cej.2023.145297
Received 29 June 2023; Received in revised form 3 August 2023; Accepted 7 August 2023
Available online 9 August 2023

Semiconductor materials are the most commonly used in TE devices, presenting high-performance but limited mechanical characteristics [13], high-cost manufacturing, and being difficult to implement by additive manufacturing technologies for easy and low-cost integration into devices [13,14]. TE ceramics are manufactured by processes involving high temperatures, expensive equipment and are not suitable for being implemented on flexible substrates [15,16]. The ZT of bulk TE materials is higher for bismuth telluride (Bi_2Te_3), lead telluride (PbTe) and bismuth sulfide (Sb_2Te_3), which are the most commonly used semiconductors for thermal energy harvesting [17–19]. Further, the abundance of bismuth sulfide (Bi_2S_3) makes it an excellent choice [19], although it presents a much lower ZT than the other indicated materials. The highest-performance materials reach near ZT ≈ 1.5 for complex or earth-rare materials [18]. Further, another relevant parameter is the optimum working temperature, which can range between 200 and 1000 K [14,18]. The Bi_2Te_3, Sb_2Te_3, Bi_2S_3 and PbTe bulk materials present a ZT ≈ 1 at 400 K [18], ZT ≈ 0.5 at 500 K [20], ZT ≈ 0.14 at 570 K [21] and ZT ≈ 0.8 at 600 K [18], respectively. Enhancing the performance of TE materials in order to increase energy harvesting efficiency is still challenging due to the interrelation between the different TE parameters. The major approach is to tailor the thermal conductivity by controlling the electrical conductivity by doping, alloying [22] or through complex and nanostructured material development. These traditional thermoelectric materials have been extensively evaluated for applications developed by additive manufacturing on flexible substrates [23]. TE devices have been developed for wide temperature range applications, using ceramic or polymeric substrates as support materials for the different TE semiconductor fillers [11,14]. Output voltages and power up to 2200 mV and 460 μW, respectively [14], have been reported, as well as PF ~2.1 mW m^{-1} K^{-2}, ZT ~0.61 at room temperature [23] and a power density up to 3.8 mW cm^{-2} [24]. The direct comparison of TE energy harvesting devices is quite complicated due to the use of different materials and filler contents in composites, varying geometries, and different numbers of p-n thermocouples. Further, literature also shows large variations on temperature ranges, application methods, and electronic circuit design, among other parameters.

The incorporation of TE ceramic fillers into polymeric matrix is one of the most suitable ways to develop robust thermoelectric devices to be integrated into portable and wearable systems to enable the supply of electronic devices from human body heat, as an example [25,26]. Devices with high thermoelectric performance have been developed based on conductive materials, such as poly(3,4-ethylenedioxythiophene): polystyrene sulfonate (PEDOT:PSS) or polyaniline (PANI) or carbon nanotubes (CNT), together with the aforementioned ceramic materials [25,27]. Conductive fillers allow for an increase in the figure-of-merit of the TE composites, which, together with the Seebeck coefficient, is the main parameter to evaluate the materials' performance [25]. Conductive polymers are largely used in TE devices and are mostly fabricated through solution methods, such as drop-casting or printing techniques [25,28]. PEDOT:PSS and PANI reinforced with TE filler present values in the order of PF = 0.38 mW m^{-1} K^{-2} and ZT = 0.32 in composites developed by solution mixing [28]. These values are lower when compared with other TE fillers, as previously indicated. TE devices based on conductive PANI/Bi_2S_3 nanorods (n-type) present a Seebeck coefficient of S = 42.8 μV K^{-1} and PF = 0.07 μW m^{-1} K^{-2} at room temperature [29]. The composite was used as a n-type material, which, together with PANI/Te as a p-type component, leads to an energy harvesting output voltage of V_{out} = 141.4 mV at ΔT = 90 °C for 7 thermocouples, with 224.4 μV K^{-1} per thermocouple [29].

For mass production of electronic devices, printing technologies are among the most promising fabrication methods [30,31] based on their low-temperature and vacuum-less processing, low-cost equipment, low material waste, and suitability for flexible substrate applications [32]. Additive manufacturing technologies have been extensively applied in the areas of printing electronics [33], sensors, and actuators [34], but are more scarce in the development of energy harvesting systems [6]. As previous mentioned, printed thermoelectric energy harvesting devices are typically achieved by combining a polymeric matrix with semiconductor materials [10]. The major advantage of composite material developments, in addition to the mechanical properties, is the possibility to print these devices using additive manufacturing, allowing optimization of the geometry and structure of the thermoelectric devices, which is also critical to enhancing their performance, based on theoretical simulations [35]. Different printing technologies, such as dispenser and screen printing for rapid and large-area applications, and inkjet or aerosol printing for high-resolution applications, have been used to produce different energy harvesting systems [36], mainly from solvent solutions [36]. As relevant examples, a printed prototype fabricated by the dispenser method has been developed based on 50 thermocouples of Bi_2Te_3 (n-type) and Sb_2Te_3 (p-type) embedded into a binder resin, leading to a power density of 75 μW cm^{-2} at ΔT = 20 °C [37]. Screen-printed TE systems with 15 thermocouples were developed based on PVDF reinforced with potassium counterion (poly[K_x(Ni-ett)]) as n-type and PEDOT:PSS/Te nanowires as p-type materials, reaching a PF ≈ 1.5 μW m^{-1} K^{-2}, V_{out} ≈ 85 mV and P_{out} ≈ 25 nW at ΔT = 45 °C [38]. A TE device with PEDOT:PSS/Bi_2Te_3 (n-type) and PEDOT:PSS/Sb_2Te_3 (p-type) materials in the form of 15 thermocouples allowed to reach a power density of 1.22 mW cm^{-2} at (ΔT = 50 °C) [39]. The highest value of power density for printed thermoelectric energy harvesting prototypes, 55 mW m^{-2} (ΔT = 70 °C), has been obtained using a composite of polystyrene with carbon nanotubes as p-type material), the PF being 0.15 μW m^{-1} K^{-2} [40].

To develop easy processing and flexible energy harvesting materials to convert thermal into electrical energy, host polymer selection is also critical for achieving both processability (e.g. by additive manufacturing) and high-performance composites but has been barely addressed. Electroactive polyvinylidene fluoride (PVDF) and its copolymers present the highest electroactive properties among polymers with good mechanical, thermal, and chemical stabilities [41,42] showing exceptional applicability as energy harvesting systems [43–45]. To achieve materials with large deformation capabilities, with up to 100% of maximum strain, a chemically stable thermoplastic elastomer composed of styrene-ethylene/butylene-styrene (SEBS) [46] has also been used for polymer composite development. In this work, PVDF and SEBS composites are proposed as polymer matrices reinforced with different types and contents of thermoelectric fillers (n- and p-type) to develop and optimize material characteristics for the implementation of thermoelectric energy harvesting systems. Further, the effect of the addition of carbon nanotubes on the electrical conductivity of the composites and TE device performance has been assessed.

2. Materials and methods

2.1. Materials

Styrene-ethylene/butylene-styrene (SEBS) with reference 108C and 85/15 ethylene-butylene/styrene ratio was supplied by Dynasol Elastomers, S.A (Spain). Poly(vinylidene fluoride) (PVDF) with reference Solef 6010 and a density of 1.75–1.8 kg/m^3 was supplied by Solvay. As semiconductor reinforcing fillers were used bismuth sulfide (Bi_2S_3) with a density of 7.7 g/ml, bismuth telluride (Bi_2Te_3) with a density of 7.6 g/ml, and antimony telluride (Sb_2Te_3) with a density of 6.5 g/ml, obtained from Sigma Aldrich. Multiwalled carbon nanotubes (CNT) with a purity of 90%, outer mean diameter of 9.5 nm, and length of 1.5 μm were supplied by Nanocyl with the reference NC7000. The solvents used to dissolve SEBS and PVDF were cyclopentyl methyl ether (CPME), from Carlo Erla (ρ = 0.86 g/cm^3 at 20 °C and a boiling temperature of 106 °C) and N,N-dimethylformamide (DMF) from Merck (ρ = 0.94 g/cm^3 at 25 °C, boiling temperature of 153 °C), respectively.

2.2. Preparation of the composites

The SEBS and PVDF polymers and composites were prepared using a polymer/solvent ratio of 1 g to 6 ml. The preparation of composites starts by placing the solvent and the corresponding filler contents (Table 1) in a glass flask for 2 h in an ultrasonic bath at 25 °C for homogeneous dispersion of the fillers. The polymer powder was then added to the aforementioned dispersion, which was magnetically stirred for 4 h at 30 °C until complete polymer dissolution. Neat SEBS and PVDF samples were produced by the same experimental procedure, except for the ultrasonic bath step, with the same polymer/solvent ratio. Finally, flexible thin films (thickness between 40 and 60 μm) were obtained by spreading the solution on a clean glass substrate and solvent evaporation. For the SEBS samples, the evaporation was at ambient temperature for 12 h and while for the PVDF solvent evaporation occurred at 210 °C for 15 min (melting and re-crystallization procedure [41]) in an oven (JP Selecta, model 2005165)). Table 1 summarizes all the samples.

2.3. Samples characterization

2.3.1. Morphological, chemical and thermal properties

The surface morphological characteristics of the samples were obtained by scanning electron microscopy (SEM) using a NanoSEM-FEI Nova 200 (FEG/SEM) at 500× and 2500× magnification. Energy dispersive X-ray analysis (EDX) was carried out at 500× of magnification to evaluate the nanofillers dispersion. Before the analyses, the samples were coated with a thin gold layer (≈10 nm) using a sputter coating (Polaron SC502).

The chemical characteristics were evaluated by Fourier-transform infrared spectroscopy (FTIR) in attenuated total reflectance mode (ATR) using Jasco FTIR-4100 equipment. A measurement resolution of 4 cm^{-1} was used in a range of 600–4000 cm^{-1} with 64 scans. Differential scanning calorimetry (DSC) tests were carried out to evaluate the thermal transitions. The heating scans were performed from −70 to 200 °C at a rate of 10 °C/min.

2.3.2. Mechanical properties

The tensile mechanical properties were evaluated with a Shimadzu model AG-IS with a load cell of 50 N. Rectangular samples (15 × 20 mm^2 and thickness between 20 μm and 60 μm) were evaluated at room temperature in the tensile mode at a deformation speed of 5 mm/min and 1 mm/min for SEBS and PVDF samples, respectively. Young modulus was determined for strains up to 10 % and 0.5 % of SEBS and PVDF, respectively.

2.3.3. Electrical and thermal conductivity

The surface electrical resistance was calculated from the slope of the I-V curves measured with a Keithley 6487 picoammeter/voltage source at room temperature. Two rectangular (10 mm length × 5 mm width) parallel electrodes were coated at a distance of 20 mm using conductive silver ink (Agar Scientific, AGG3790). The electrical conductivity (σ) was calculated using also geometrical factors of the samples, length (l) and distance (d) of electrodes.

$$\sigma = \frac{1}{R}\frac{d}{l} \quad (1)$$

The electrical resistance was calculated at room temperature and in the temperatures range between 30 and 150 °C in 20 °C intervals. The temperature was first stabilized for 2 min and the I-V slope was measured 3 consecutive times.

Dielectric measurements were performed at room temperature using a Quadtech 4000 model to record the capacity and tan δ in the frequencies range between 200 Hz and 1 MHz. The dielectric constant was obtained considering the sample geometry and the parallel plate condenser measurement geometry (parallel gold electrodes with a diameter of 5 mm deposited with a Polaron SC502 sputter coater).

The thermal conductivity (k) (W/(m·K)) was calculated using the Eq. (2):

$$\kappa = \rho \times \alpha \times C_p \quad (2)$$

where ρ is the density, α the thermal diffusivity and C_p the specific heat capacity. The samples were previously sprayed to coating with graphite and cut into squares with 8 mm. The density of the samples was measured according to ISO 1183 using a hydrostatic balance. Thermal diffusivity was measured at 25, 50, 75, and 100 °C using a thermal analyzer (LFA 447 Nanoflash Netzsch, Germany). The diffusivity data was obtained by pulse corrected by the Cowan model. The specific heat capacity data was obtained by DSC 2010 CE calorimeter (TA Instruments) according to ISO 11357 using sapphire as standard.

2.3.4. Thermoelectric properties

The thermoelectric effect was evaluated by determining the Seebeck coefficient defined as $S = \Delta V/\Delta T$, where ΔV is the potential difference measured when a gradient of temperature (ΔT) is applied. ZT is defined as $ZT = S^2\sigma T/\kappa$, for a given temperature, and the power factor is defined as $PF = S^2\sigma$. A homemade platform was developed that allows varying temperatures, ensuring the thermal gradient along the sample length. The developed system is based on two Peltier devices, in which the cells are placed with an opposite potential difference (positive and negative), and an aluminum base is attached to the surface of the Peltier plate (TEC1-12705, 12 V, 5 A Qcma, 30 W, Δt_{max} 61 °C), for improving temperature homogeneity (Fig. 1).

On the lower surface of the Peltier plates, a water-cooling system with an independent control was placed, allowing to optimize the thermal difference between the aluminum plates, controlled by a temperature sensor (PT100- 32209210 from Nexensos) placed on the aluminum plate. An electronic power system was also developed to control the potential difference in the Peltier plates, activating the cooling system, and reading the temperature sensor data. The electronic control system is based on an ESP32-C3 microcontroller (from Espressif Systems), with BLE communication, allowing interaction with the device. The control of the Peltier plates is achieved with a relay bridge, enabling independent control of the two plates and the refrigeration system according to the applied stimulus. PT100 temperature sensors were used, connected to a Wheatstone bridge. A differential amplifier INA122P (Texas Instruments) was applied to the bridge terminals and its output was connected to the analog to digital converter (ADC) of the microcontroller, allowing the recording of temperature over time. The entire structure of the system was built using commercial polytetrafluoroethylene (PTFE), allowing the two chambers with different temperatures, according to Fig. 1A.

Table 1
Samples prepared and corresponding nomenclature.

Polymer	Filler	Weight percentage (wt.%)	Sample nomenclature
PVDF	–	–	PVDF
	Bi_2S_3	30	PVDF/30Bi_2S_3
	Bi_2S_3/CNT	50	PVDF/50Bi_2S_3
		80	PVDF/80Bi_2S_3
		49 + 1	**PVDF/CNT/Bi_2S_3**
	Bi_2Te_3	50	PVDF/50Bi_2Te_3
	Bi_2Te_3/CNT	**49 + 1**	**PVDF/CNT/Bi_2Te_3**
	Sb_2Te_3	50	PVDF/50Sb_2Te_3
SEBS	–	–	SEBS
	Bi_2S_3	50	SEBS/50Bi_2S_3

2.4. Thermoelectric theoretical model

A TE energy harvesting model was developed to predict the output voltage, current, and power generated based on Finite Elements Methods (FEM) [47–49]. The TE energy harvesting performance was

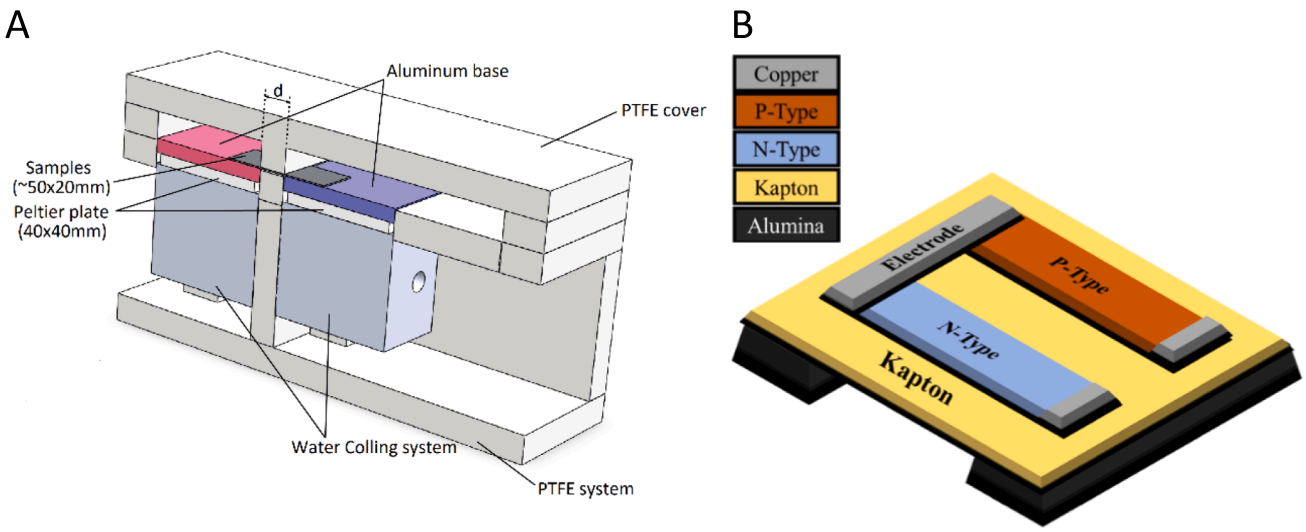

Fig. 1. A) Homemade system using two commercial Peltier systems to evaluate the thermoelectric response. B) Structure of a thermoelectric energy harvesting device with 1 thermocouple. The materials dimensions are summarized in Table SI4.

evaluated under several temperature gradients and for a different number of thermocouples and the generated voltage and current were calculated using the constitutive equations described in Table SI1 and SI2 on Supporting information (SI4 section) [47]. The theoretical model was based on the structure of the samples produced experimentally with PVDF/50Bi_2S_3 and PVDF/50Bi_2Te_3 as TE materials and copper as electrodes, as represented in Fig. 1B.

The performance of the thermocouples under several temperature gradients was evaluated using the model equations, boundary conditions, and main parameters to characterize the TE materials summarized in Table SI3 and SI4 of the SI4 section.

3. Results and discussion

3.1. Morphological, chemical and thermal properties

The cross-section morphology of PVDF, SEBS, and corresponding composites was characterized by SEM and EDX techniques (Figs. 2 and 3). Fig. 2 shows a suitable dispersion of the different TE fillers within the host polymer matrices, with individual filler dispersion and some agglomerates, critically related to filler size. Further, the materials show a compact structure without holes or voids, for all materials. The average diameter of the TE clusters is about 10 μm, although some cluster sizes go up to 20–25 due to larger particle diameters (mainly for Bi_2Te_3 filler). The CNTs are not observed, as the size and amount are much lower than the TE fillers.

There are no differences between composites and ternary composite structures and filler dispersion, independently of the polymer matrix and the filler type. In all cases, it can be observed a homogeneous filler dispersion for lower-size particles and some agglomerates of the larger particles. The distribution of the fillers is also evidenced by the EDX images presented in Fig. 3. Chemical elements such as bismuth (Bi), sulfur (S), tellurium (Te) or antimuonium (Sb) are well distributed, although some larger particles are observed for the majority of the composites. As observed in the SEM images, the filler characteristics are critical in the proper dispersion and distribution within the host polymer, independently of whether the polymer is SEBS or PVDF.

FTIR analysis was performed to obtain the vibrational spectra of the

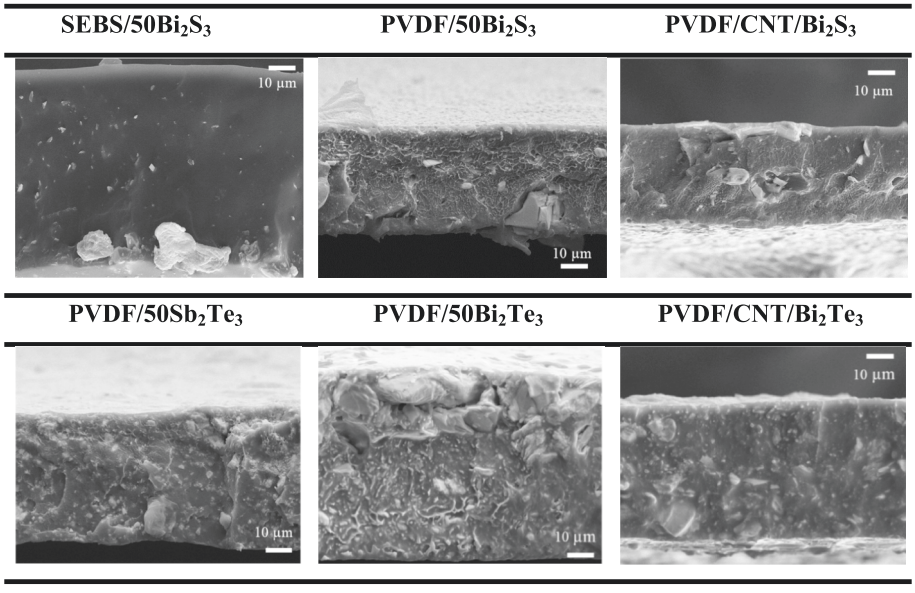

Fig. 2. Cross-section SEM images at 2500× of magnification for the processed composites with 50 wt% filler content and for the ternary composite with 1% CNTs.

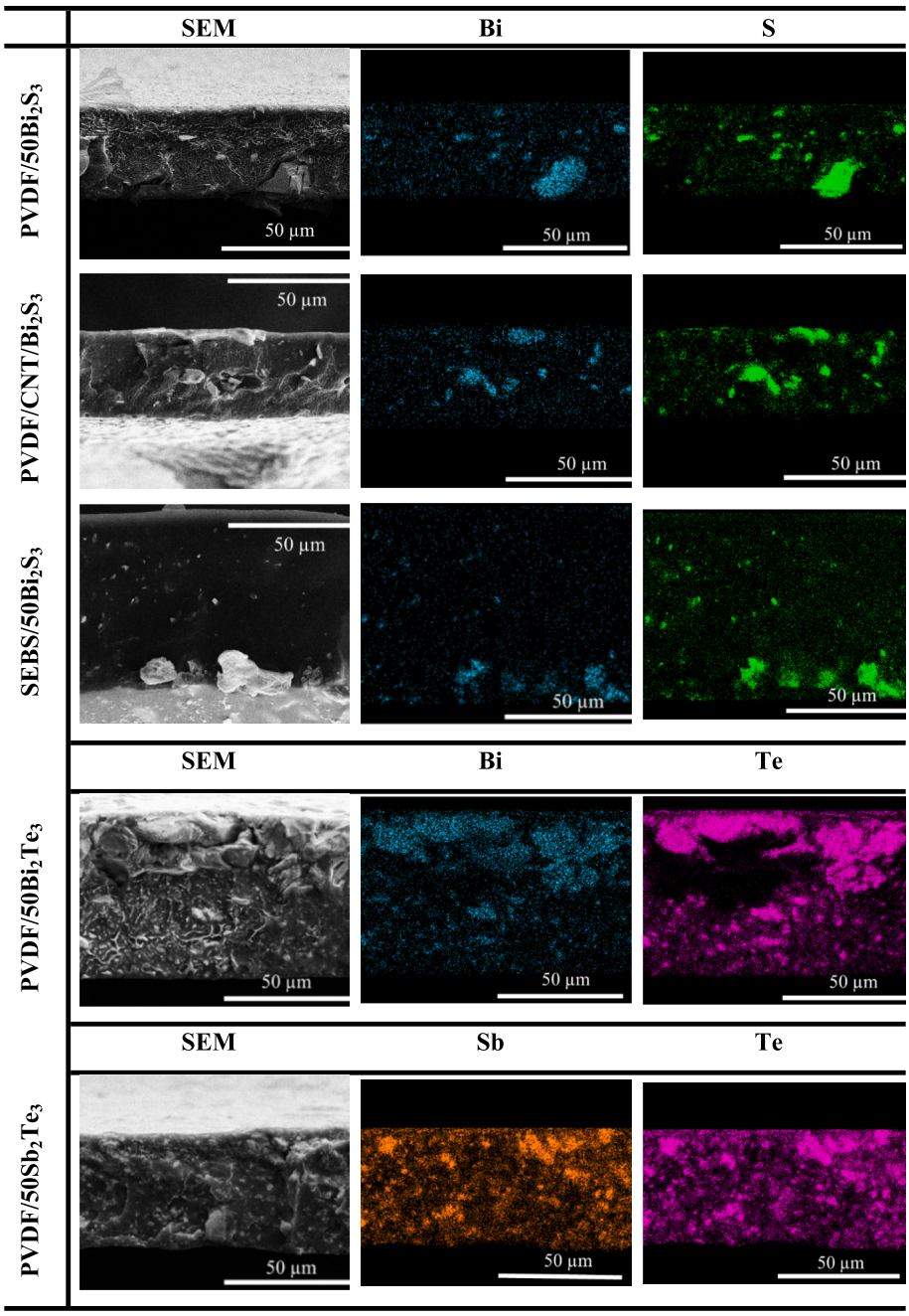

Fig. 3. Cross-section SEM and EDX images at 500× of magnification for the composites using PVDF and SEBS as matrices and TE fillers.

samples and the possible chemical interactions between the polymeric matrix and the fillers. Fig. 4A shows the FTIR spectra for pristine PVDF and SEBS and their respective composites. For the neat PVDF, vibrations corresponding to the α-phase are observed at 614 cm^{-1} and to the γ-phase at 833 cm^{-1} [41]. In the processed PVDF and composites, peaks of the γ-phase are also found at 833 and 1233 cm^{-1}. The composites that contain bismuth show a similar band structure as PVDF, while the PVDF/50Sb_2Te_3 almost inhibits the γ-phase in the sample, and presents pronounced α-phase peaks at 766 and 976 cm^{-1} [41]. Thus, PVDF and composites crystallize mainly in the non-polar α-phase with some traces of the polar γ-phase, independently of the filler, except for the 50Sb_2Te_3/PVDF composite. The crystallization temperature plays an important role in determining polymer phase crystallization in the case of PVDF. For solution-processed PVDF, solvent evaporation above the melting temperature of the polymer typically leads to polymer crystallization mainly in the non-polar α-phase, except for particular cases in which strong polymer-filler interactions lead to polymer crystallization in the polar phases [50].

Fig. 4B, shows that both, neat SEBS and the SEBS/50Bi_2S_3 composites, present absorption bands characteristic of styrene (at 699 cm^{-1} [46]) and butadiene. In particular, the absorption peaks in the 3000–2800 cm^{-1} region are associated with the C-H aliphatic groups [46], and the aromatic C = C stretching of styrene peaks is located at 1454 cm^{-1} [46]. The ring out-of-plane deformation vibration peak was also observed from the aliphatic C-H bending, at 1373 cm^{-1} [51]. For both PVDF and SEBS-based composites, the inclusion of the fillers does not affect the characteristic absorption bands of the respective polymers and no new bands are observed, indicative of chemical interactions between filler and polymer host.

Fig. 4C and D show the DSC thermograms of the PVDF and SEBS-

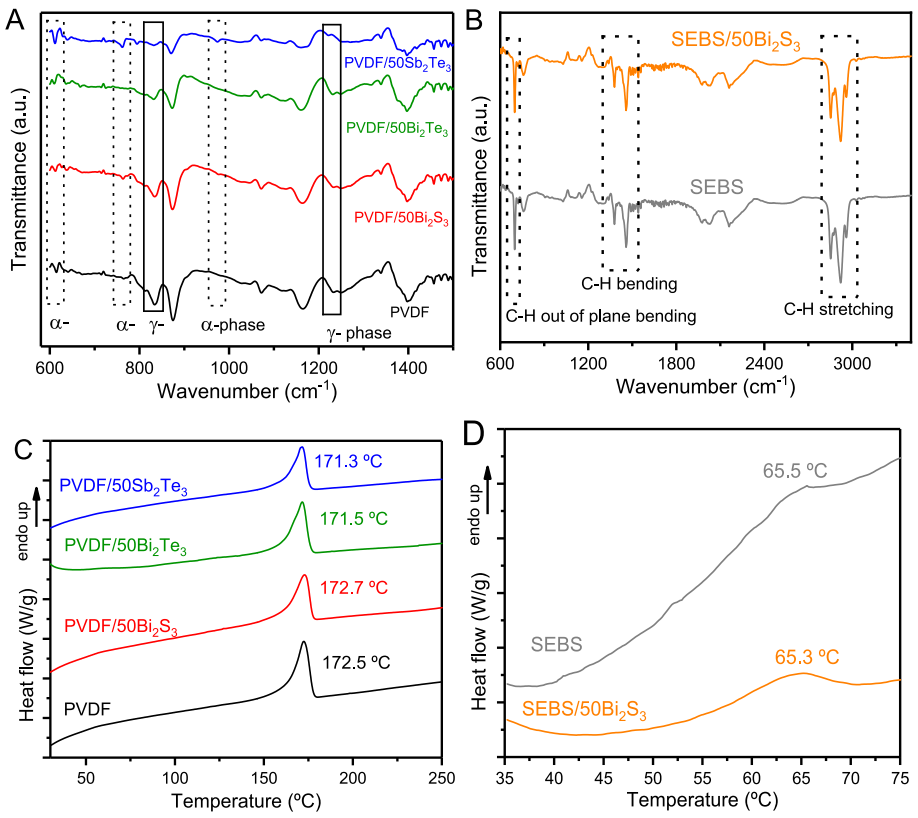

Fig. 4. FTIR spectra of the pristine polymers and corresponding composites for PVDF (A) and SEBS (B). DSC analysis of the samples based on PVDF (C) and SEBS (D).

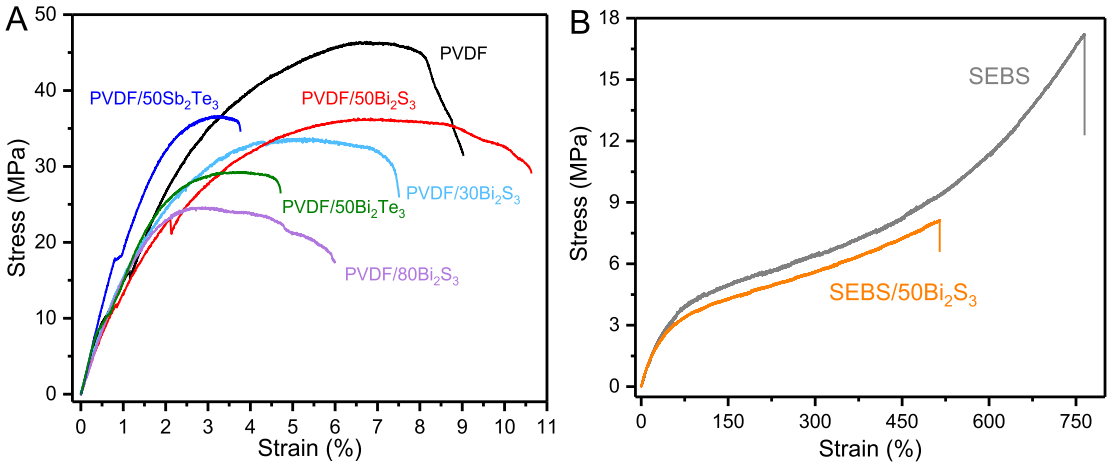

C Samples	Young Modulus (GPa)	Samples	Young Modulus (GPa)
PVDF	1.9 ± 0.4	**PVDF/50Bi$_2$Te$_3$**	1.8 ± 0.3
PVDF/30Bi$_2$S$_3$	1.8 ± 0.3	**PVDF/CNT/Bi$_2$Te$_3$**	1.9 ± 0.4
PVDF/50Bi$_2$S$_3$	1.6 ± 0.3	**PVDF/50Sb$_2$Te$_3$**	2.1 ± 0.3
PVDF/80Bi$_2$S$_3$	1.8 ± 0.3	**SEBS**	8.2 ± 0.9 **(MPa)**
PVDF/CNT/Bi$_2$S$_3$	1.6 ± 0.4	**SEBS/50Bi$_2$S$_3$**	10.8 ± 1.0 **(MPa)**

Fig. 5. Representative tensile stress–strain curves of PVDF (A) and SEBS composites (B). C) Young modulus for the different polymer and polymer composites.

based samples, respectively. PVDF and composites with 50 wt% filler content show similar melting temperatures, about 171–173 °C, in agreement with the literature [41] for α-PVDF (167–172 °C). The glass transition temperature of SEBS and SEBS/50Bi_2S_3 also occurs at the temperature of 65 °C, related to the polystyrene glass transition [52]. The glass transition of the polybutadiene is found at lower temperatures, around 10 °C or lower [53,54], depending on the copolymer ratio [53]. Similar to both matrices, the inclusion of the different fillers does not lead to relevant variations in the thermal transitions of the matrixes, demonstrating that the pristine polymer determines the temperature range for devices such as TE generators.

3.2. Mechanical properties

The mechanical properties of thermoplastic PVDF, elastomeric SEBS and the corresponding composites are presented in Fig. 5. PVDF shows a typical thermoplastic behavior in the quasi-static uniaxial stress–strain measurements (Fig. 5A), with strain at a break of around 8%. The composites reinforced with Bi_2S_3 present similar performance for 30, 50 and 80 wt% filler content, with strain at a break between 6 and 11%, decreasing for PVDF/50Bi_2Te_3 and PVDF/50Sb_2Te_3 to near 4 to 4.5% of strain. The stress at break changes between 20 and 35 MPa, where the PVDF presents the highest value. Larger filler content and micrometer sizer of fillers (observed in Figs. 2 and 3) leads to a decrease in the overall mechanical properties due to weak filler-polymer interfaces [55]. In any case, independently of the filler content, the composites remain flexible and easy to handle, making them suitable for thermoelectric applications. For stretchable applications, the use of SEBS is more suitable as it withstands large strains [46]. Fig. 5B shows the elastomeric behavior of neat SEBS and composite, where the maximum strain is near 750% for the pristine polymer, decreasing to 470% for the composite with a 50 wt% content of Bi_2S_3. Both materials present excellent maximum strain, and the stress at break decreases for the composite due to the defective sited for mechanical deformation that represents the filler-polymer interfaces. The Young modulus measured at 1% strain for PVDF and at 10% strain for SEBS is shown in Fig. 5C. The Young modulus is near $E \approx 1.9$ GPa for PVDF and is similar for most of the composites, with a slight increase for the PVDF/50Sb_2Te_3 composite. For elastomer SEBS and SEBS/50Bi_2S_3 composite, the Young modulus is ~200× lower than PVDF materials, ranging between $E \approx 8$ and 10 MPa, respectively.

3.3. Electrical and thermal conductivity

The electrical conductivity of PVDF, SEBS, and their composites is represented in Fig. 6A. In the case of neat SEBS and PVDF samples, the electrical conductivity is 1.8×10^{-10} $(\Omega{\cdot}m)^{-1}$, as it corresponds to electrically insulating materials [42]. The reinforcement with Bi_2S_3 fillers leads to a slight increase in the conductivity (≈$2.2–4.1 \times 10^{-10}$ $(\Omega{\cdot}m)^{-1}$) for both SEBS and PVDF when compared to the neat samples. In the case of PVDF/Bi_2S_3 composites, the electrical conductivity is nearly independent of the filler content. Further, the inclusion of Bi_2Te_3 does not lead to significant variation of the electrical conductivity, with the PVDF/50Bi_2Te_3 samples showing similar conductivity values to the neat PVDF samples. On the other hand, the inclusion of Sb_2Te_3 with 50 wt% content into the PVDF matrix leads to a strong increase of the conductivity in four orders of magnitude, up to 5.67×10^{-6} $(\Omega{\cdot}m)^{-1}$, leading therefore to a semiconducting composite, which will influence the TE efficiency [56].

Moreover, the inclusion of CNT (1 wt%) into PVDF reinforced with Bi_2S_3 and Bi_2Te_3 leads to a strong increase in the electrical conductivity of 11 and 10 orders of magnitude for Bi_2S_3 and Bi_2Te_3, respectively (patterned bars in Fig. 6A), with respect to the pristine polymer as reported by literature for PVDF is above the percolation threshold [42].

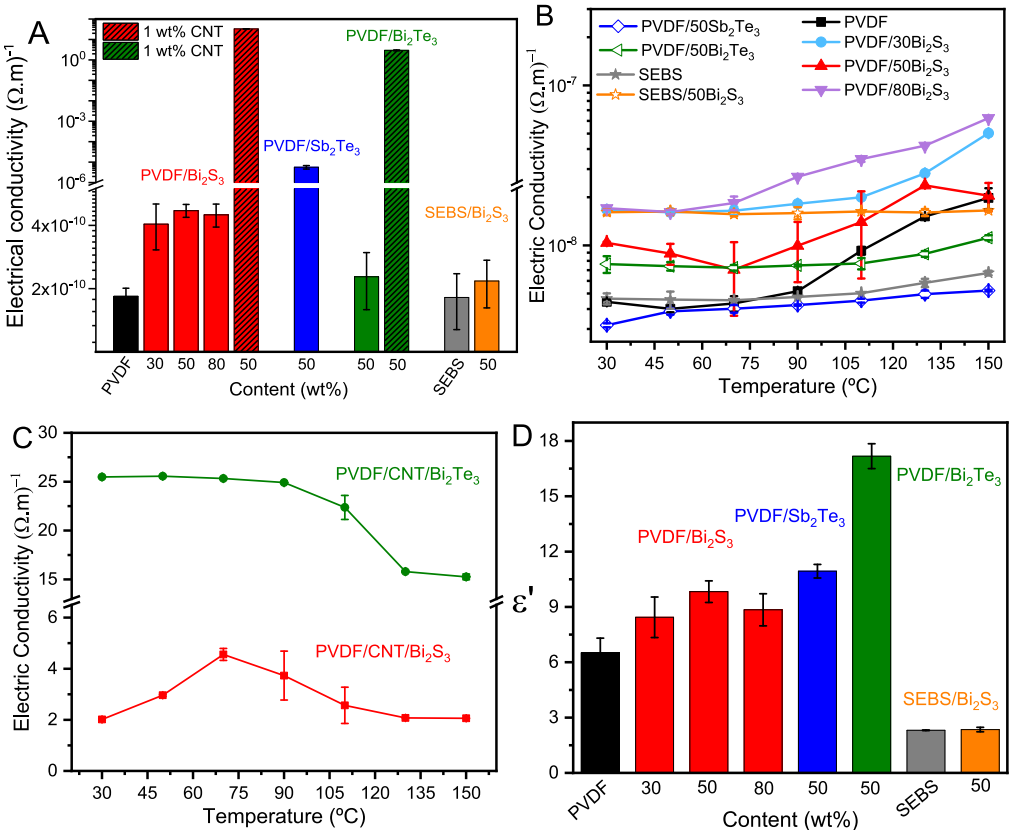

Fig. 6. Electrical conductivity of the pristine PVDF, SEBS and composites at room temperature (A) and in function of the temperature for composites (B) and for the ternary PVDF based composites (C). Dielectric constant of composites at 1 kHz (D).

Thus, the ternary composites become electrically conductive.

Further, the dependence of the electrical conductivity on temperature is shown in Fig. 6B and C. The PVDF composites show an increase in electrical conductivity as the temperature increases (Fig. 6B). This effect is particularly relevant for temperatures higher than 100 °C, above the α-relaxation of the semicrystalline polymer [57], with the electrical conductivity increasing from 5×10^{-8} to 1×10^{-7} $(\Omega \cdot m)^{-1}$ from 90 to 150 °C, respectively. This behavior is characteristic of PVDF, independently of type and content [57,58]. Similar to PVDF composites, the SEBS/50Bi_2S_3 sample shows higher electrical conductivity than neat SEBS, but no temperature variation of the electrical conductivity is observed in the temperature under consideration. Two main factors influence the overall electrical conductivity in polymer composites as a function of temperature: on the one hand, increasing temperature leads to an increase of energy and mobility of the electrons, which are activated for electrical conduction [59,60] and, on the other hand, the ions of the conductive fillers oscillate about their mean positions colliding more frequently with the electrons, reducing the electrical conductivity [59,60].

Lastly, Fig. 6C shows the temperature dependence of the electrical conductivity in the ternary composites, the electrical conductivity of PVDF/CNT/Bi_2Te_3 decreases with increasing temperature, whereas the electrical conductivity of PVDF/CNT/Bi_2S_3 is stable in the present temperature range. Both conductive samples show among the highest electrical conductivity for thermoelectric polymer/CNT based samples [61].

The dielectric response of the composites at room temperature demonstrates that the dielectric constant (measured at 1 kHz) of PVDF is about $\varepsilon' \approx 6.5$, increasing slightly for composites with different filler types or content. The composites show dielectric constants typically between 8 and 12, the highest dielectric constant being obtained for the Bi_2Te_3 based sample reaching values of $\varepsilon' \approx 17$, three times higher than for neat PVDF (Fig. 6D). This dielectric response of pristine PVDF agrees with the literature [41,62], as well as the corresponding increase with the introduction of the fillers, an increase that is determined by both filler type and content [63]. The addition of CNTs makes composites electrically conductive, without the ability to store electrical energy. SEBS presents a lower dielectric constant than PVDF, being near $\varepsilon' = 2.3$ for both pristine SEBS and composite [46], mainly due to the poor filler-matrix interactions and the vacancies or pores created in the structure [55]. The frequency dependent dielectric constant is shown in Figure SI3, the behavior being similar for all samples and in line with the response of the pristine polymer [64].

3.3.1. Thermal conductivity

The thermal conductivity for neat PVDF, SEBS, and composites at different temperatures is represented in Fig. 7. The thermal conductivity is less influenced by temperature than the electrical conductivity, and in composites, it strongly depends on filler-filler and filler-polymer interfaces and interactions [65]. The thermal conductivity of PVDF is about 0.03 W/(m·K), being stable in the temperature range from 25 to 100 °C, and increasing with the introduction of the fillers, as shown in Fig. 7A [66]. The larger increases in thermal conductivity occur for the Bi_2Te_3 containing samples with a thermal conductivity ranging between $0.15 < k < 0.18$ W/(m·K), about 5× higher than for neat PVDF. The remaining PVDF composites show a thermal conductivity 2× higher than the neat polymer. The further inclusion of the CNTs leads to a reduction of the thermal conductivity in the ternary composites with respect to the composites with the semiconductive fillers. The heat in the semiconducting system is carried by photons, which are easier scattered in composite materials with distinct elastic properties [67]. Neat SEBS and composites show lower thermal conductivity when compared to PVDF, as shown in Fig. 7B. In fact, semicrystalline thermoplastic polymers present higher thermal conductivity than amorphous elastomers [68]. The parameters that influence the thermal conductivity, including the specific heat capacity and the thermal diffusivity, were evaluated at several temperatures, as represented in Fig. SI4.

By comparing with the literature [61,65], the polymer composites show low thermal conductivity, which is suitable for their applicability in TE harvesting devices, once to increase the ZT value, the thermal conductivity needs to be as low as possible.

3.4. Thermoelectric properties

The TE properties of the composites are represented in Fig. 8, with a distance between the two Peltiers of d = 30 mm (see Fig. 1A) and an average temperature of 58 °C, to maximize the heat flow through the composites. PVDF/Bi_2S_3 composites show the Seebeck coefficient increasing from 15 to 25 and 36 μV/K, respectively for 30, 50, and 80 wt % filler content. This increase is related to the intrinsic Seebeck coefficient of the TE fillers, depending on whether they are p- or n-type can vary from 90 to 160 μV/K [23,24,39,69,70]. This TE performance agrees with the reported literature on TE or conductive fillers embedded in PVDF-based composites, where Seebeck coefficients ranging from 10 and 35 μV/K [26,71,72] have been reported. When considering the same content of p-type fillers in PVDF/50Sb_2Te_3 and PVDF/50Bi_2Te_3 composites, it is shown that the PVDF/50Bi_2Te_3 samples show a higher value (29 μV/K) when compared to the sample PVDF/50Sb_2Te_3 (15 μV/K).

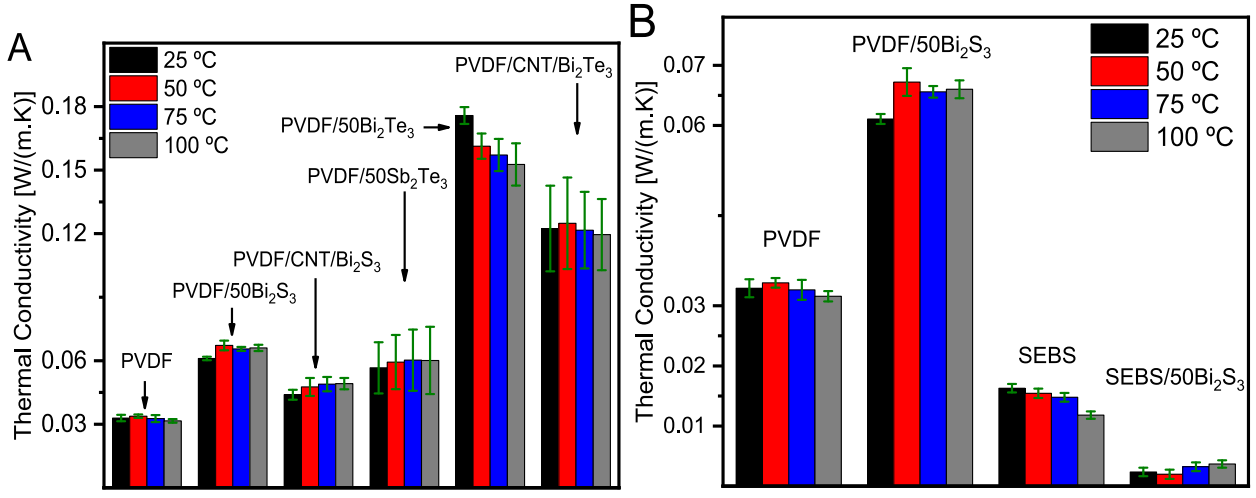

Fig. 7. Thermal conductivity at different temperatures for PVDF and composite samples (A). Comparison of SEBS and PVDF neat and composite samples for the same filler content (B).

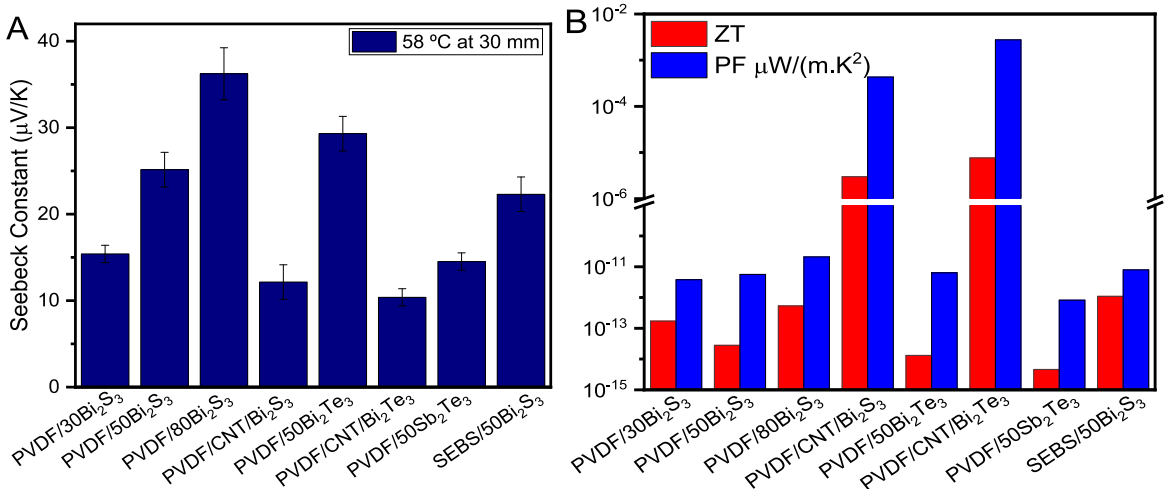

Fig. 8. (A) Seebeck coefficient as a function of filler type and content and (B) ZT and PF for the PVDF, SEBS and respective composites as a function of filler type and content at average temperature of 58 °C at 30 mm of distance.

Thus, bismuth tellurium presents higher TE performance in composites, even though presents a composite with higher dielectric constant or thermal conductivity and lower electrical conductivity. The ternary composite sample presents larger electrical conductivity but a lower Seebeck coefficient for PVDF/CNT/50Bi_2S_3 and PVDF/CNT/50Bi_2Te_3 composites, decreasing to one-half and one-third, respectively. As reported in the literature, the conductive carbonaceous fillers present lower Seebeck coefficients (from 10 to 20 μV/K for CNT/PVDF composites [26,73]). In general, higher electrically conductive materials present lower Seebeck coefficients [26,72–74], and higher thermal conductivity composites presents larger Seebeck value. The relative content of crystalline and amorphous phases can also play a relevant role in the Seebeck coefficient of the samples, as it influences charge carrier mobility [74]. In the case of the SEBS matrix, the n-type composites based on SEBS/50Bi_2S_3 showed a Seebeck coefficient of 22.3 μV/K, slightly lower when compared to the PVDF/50Bi_2S_3 composite with 25 μV/K. Between both, semicrystalline PVDF presents a slightly higher Seebeck coefficient than the elastomer SEBS. Thus, the Seebeck coefficient is more influenced by the specific filler than by the intrinsic properties of the polymer matrix.

The figure-of-merit and power factor at $\Delta T = 58$ °C is presented in Fig. 8B. PVDF reinforced with Bi_2S_3 slightly increases the PF from 3.8 to 21.0 × 10^{-12} (μW/(m·K^2)) with increasing filler content from 30 to 80 wt%, respectively. PVDF/50Bi2Te3 composites present similar performance while the Sb_2Te_3 composite presents one order of magnitude lower values for the PF parameter. Comparing both matrices reinforced with Bi_2S_3, SEBS composites present slightly higher PF values. Electrical conductivity critically influences the PF values of the composites, as can be observed for ternary composites with CNT, presenting 8–9 orders of magnitude higher values when compared with just semiconducting composites. Similar ZT performance can be observed for composites when compared to ternary materials. The PF values of the PVDF/CNT/Bi_2S_3 and PVDF/CNT/Bi_2Te_3 samples show higher PF values, being 4.3 × 10^{-4} μW/(m·K^2) and 2.8 × 10^{-3} μW/(m·K^2), respectively.

For PVDF composites, optimized PF and ZT factors reach up to 2.1 × 10^{-11} μW/(m·K^2), and 5.3 × 10^{-13}, respectively, for the 80 wt% Bi_2S_3 content composite. In relation to filler type, n-type (Bi_2S_3) and p-type (Bi_2Te_3 and Sb_2Te_3) show similar ZT values, except for PVDF/50Sb_2Te_3 due to the lower thermal conductivity. The developed materials also show similar TE values when compared with the literature for related polymer/CNT based TE materials [10,26]. The overall results of the developed materials are summarized in Table 2.

Polymer-based TE energy harvesters typically show a low Seebeck coefficient, leading to lower energy harvesting characteristics than

Table 2
Summary of the main properties of the materials for TE applications at 58 °C.

Sample	σ (Ω·m)$^{-1}$	*S* (μV/K)	PF μW/(m·K^2)	κ W/(m·K)	ZT
PVDF	1.8 ± 0.2 × 10^{-10}	14.4	8.5 × 10^{-13}	3.4 × 10^{-2}	8.3 × 10^{-15}
PVDF/30Bi_2S_3	4.1 ± 1.0 × 10^{-10}	15.4	3.8 × 10^{-12}	7.3 × 10^{-3}	1.7 × 10^{-13}
PVDF/50Bi_2S_3	4.7 ± 0.3 × 10^{-10}	25.2	5.7 × 10^{-12}	6.7 × 10^{-2}	2.8 × 10^{-14}
PVDF/80Bi_2S_3	4.5 ± 0.6 × 10^{-10}	36.2	2.1 × 10^{-11}	1.3 × 10^{-2}	5.3 × 10^{-13}
PVDF/CNT/Bi_2S_3	32.9 ± 0.2	12.2	4.3 × 10^{-4}	4.8 × 10^{-2}	2.9 × 10^{-6}
PVDF/50Bi_2Te_3	2.3 ± 0.7 × 10^{-10}	29.3	6.4 × 10^{-12}	1.6 × 10^{-1}	1.3 × 10^{-14}
PVDF/CNT/Bi_2Te_3	2.9 ± 0.2	10.4	2.8 × 10^{-3}	1.2 × 10^{-1}	7.6 × 10^{-6}
PVDF/50Sb_2Te_3	5.7 ± 1.1 × 10^{-6}	14.5	8.2 × 10^{-13}	5.9 × 10^{-2}	4.6 × 10^{-15}
SEBS	1.8 ± 0.5 × 10^{-10}	10.6	5.2 × 10^{-13}	1.6 × 10^{-2}	1.1 × 10^{-14}
SEBS/50Bi_2S_3	2.2 ± 0.6 × 10^{-10}	22.3	7.9 × 10^{-12}	2.4 × 10^{-3}	1.1 × 10^{-12}

semiconducting materials [10,75], nevertheless, the former show advantages for large area applications, conformable and flexible surfaces, based on the insulator matrices with excellent mechanical, chemical, and thermal properties [6]. Materials similar to those developed in this work are reported in the literature (Table 3) demonstrating that the TE performance critically depends on the filler reinforcement properties and content, being developed composites where the polymer is used as binder materials (larger filler than polymer content) [76]. Such filler content strongly decreases the mechanical properties of the TE materials and, consequently, the devices applications as flexible materials able to be fabricated by additive manufacturing. Thermoelectric semiconductive fillers embedded into a polymer matrix with larger filler contents present an S ~ 100 μV/K using the polymer as a binder (higher amount of filler than polymer [67,77]), near the intrinsic Seebeck coefficient of inorganic semiconductors with <300 μV/K [18,78] and ZT < 2 [14,78]. TE composites can nevertheless be improved through doping or band gap engineering [79], as well as by processing conditions and device geometry [25]. Electrical conductivity influences significantly the ZT and PF values, while the Seebeck coefficient depends on the type of charge carriers and their mobility with temperature variations, decreasing in composites compared to pristine inorganic

Table 3
Comparison of the main characteristics of the thermoelectric polymer-based composites developed in this work, with related ones form the literature.

Matrix	Filler	S (μV/K)	PF (μV/(m·K^2))	ZT	Ref
PVDF	Ionic Liquid	26.1	–	0.75	[83]
	Bi_2Se_3	90	10^{-3}	0.5	[67]
		80	32.6	0.02	[77]
	Bi_2Te_3	273.5	133.4	–	[81]
	Cu-Bi_2Se_3	90	103	0.10	[84]
	Ag_2Se	100	180	10^{-3}	[85]
	Ni	–	31	24	[86]
	Bi_2S_3	**36**	10^{-11}	10^{-13}	**This study**
	CNT	30	22		[87]
		14	10^{-4}	10^{-7}	[88]
		14–18	10^{-5}–10^{-2}	10^{-8}–;10^{-5}	[26]
		8–12	10^{-6}	10^{-9}	[73]
	Graphene	25–58	–	–	
	Graphite	8.8	6.8	10^{-3}	[71]
	Bi_2S_3/CNT	**12**	**10^{-4}**	**10^{-6}**	**This study**
ABS	CNT	3.6	10^{-4}	10^{-7}	[88]
PS	$Bi_{0.5}Sb_{1.5}Te_3$ $Bi_2Se_{0.3}Te_{2.7}$	90	0.06	–	[89]
SEBS	**Bi_2S_3**	**22**	**10^{-13}**	**10^{-13}**	**This study**

semiconducting materials [78,80].

The energy generation using TE composites are some μA, μV in open and short-circuit, respectively, and nW of output power [81,82], which critically depends on the number of devices or temperature gradient [81], however, it is rarely studied in articles related to TE devices.

Polymer-based (most of them intrinsic conductive polymers) composites reinforced with conductive carbon-based and inorganic TE fillers demonstrate a wide range of PF and Seebeck coefficients [76], the best results for Seebeck coefficient and PF being in the order of 10^2 μV/K and 10^2 μV/(m·K^2), respectively [76].

3.5. Thermoelectric energy harvesting

Evaluating the overall results of the neat polymers and composites, summarized in Table 2, the samples with higher PF are the PVDF/50Bi_2S_3 and PVDF/50Bi_2Te_3 for n- and p-type semiconductors, respectively, excluding the ternary composites since their high PF values are due to high electrical conductivity (Fig. 6A) and not related to high thermoelectric properties (decreasing the Seebeck coefficient) of the materials as represented in Fig. 9A. To evaluate the thermoelectric energy harvesting, thermocouples, with 1 and 2 pairs, were connected and the generated output voltage was measured at 3 different temperatures (27, 85, and 100 °C) using the system represented in Fig. 1. Both n- and p-type samples used to generate energy have a width and length of 5 and 48 mm respectively, and a thickness of 45–50 μm. In Fig. 9 it is represented the thermoelectric energy harvesting characteristics of the polymer-based devices using 2 different load resistances (R_L) of 10 MΩ and 10 GΩ. The device composed of 1 thermocouple (black bars) connected to R_L = 10 MΩ showed a similar output voltage for the different temperatures, near 3.5 mV. When the device is composed of 2 thermocouples (red bars), the output voltage increases from 1.4 V to 5.1 V for temperature gradients of 27 and 100 °C, respectively. The TE voltage increases with thermocouple pairs and also increases with increasing R_L = 10 MΩ to 10 GΩ (Fig. 9A).

The generated power is represented in Fig. 9B, the output power being very similar for 1 thermocouple connected to a load resistance of 10 MΩ, near 1.3 pW. In the case of 2 thermocouples connected to an R_L = 10 GΩ, the instant power was 0.2 nW and 2.68 nW for a temperature gradient of 27 and 100 °C, respectively. These results are promising when compared with the results of the literature, with the thermoelectric energy harvesting systems being composed of several thermocouples [75,90]. The device composed of 2 thermocouples reaches 2.68 nW of power for the higher temperature gradient (100 °C) used in this work which is similar to the higher values obtained for polymer-based thermoelectric devices [75]. The time required to reach such a high output voltage is represented in Fig. 9C, for the 2 thermocouple systems at different temperature gradients. It is observed that, at a given time, the device presents a larger output voltage for larger temperature gradients. In the case of ΔT = 27 °C, the output voltage tends to stabilize after 100 s near 1 V, increasing linearly for ΔT = 85 °C at 1.5 V for 250 s, although, for the initial period, the output voltage is similar to the ΔT = 27 °C. Increasing the temperature gradient (ΔT = 100 °C) a maximum voltage near 5 V was obtained at 100 s. The strong increase of the output voltage generated for a ΔT = 100 °C is related to the electrical conductivity increase near 100 °C (Fig. 6A) [57].

3.6. Theoretical modeling

The TE energy harvesting performance of several thermocouples was evaluated in a stationary study with several temperature gradients. Simulations were performed considering a system with thermal insulation where the only source of heat is the alumina, in which the cold end temperature was fixed at 20 °C and the hot end temperature was changed to 40, 60, 80, 100, and 120 °C. The n- and p-type materials were connected with cooper electrodes as represented in Figure SI5 (in SI) then, due to the electrical insulation and current conservation, the thermoelectric materials converted the thermal to electrical energy. The two lower electrodes were connected to an electrical circuit (load resistance) to evaluate the energy harvesting performance. The equations that describe all these physical principles are summarized in Table SI1.

The thermoelectric energy harvesting performance of 1 pair is represented in Fig. 10A for a ΔT = 100 °C. In Fig. 10B the output voltage for

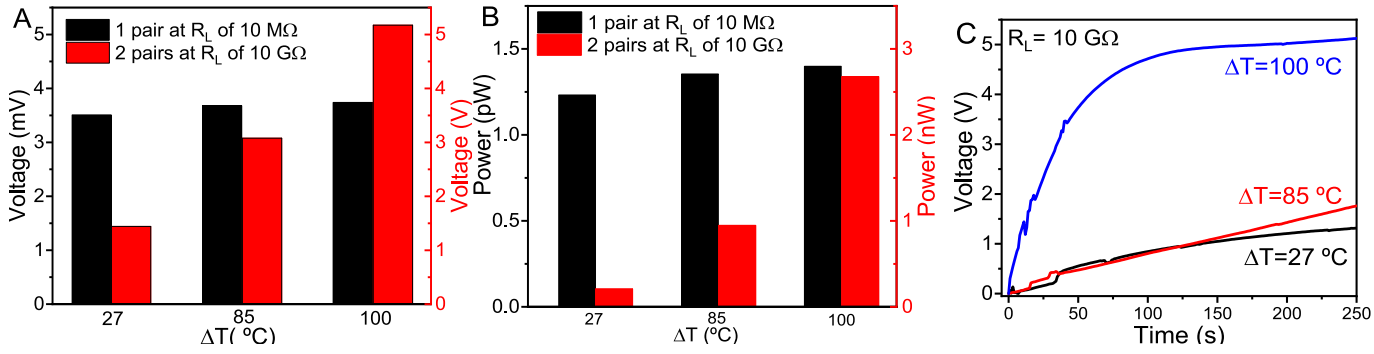

Fig. 9. TE performance of a 1 (black) and 2 (red) thermocouples (PVDF/50Bi_2S_3-PVDF/50Bi_2Te_3) for several temperature differences: A) output voltage and B) instant power for R_L = 10 MΩ and 10 GΩ. C) TE output voltage for several temperature gradients for 2 thermocouples for a R_L = 10 GΩ.

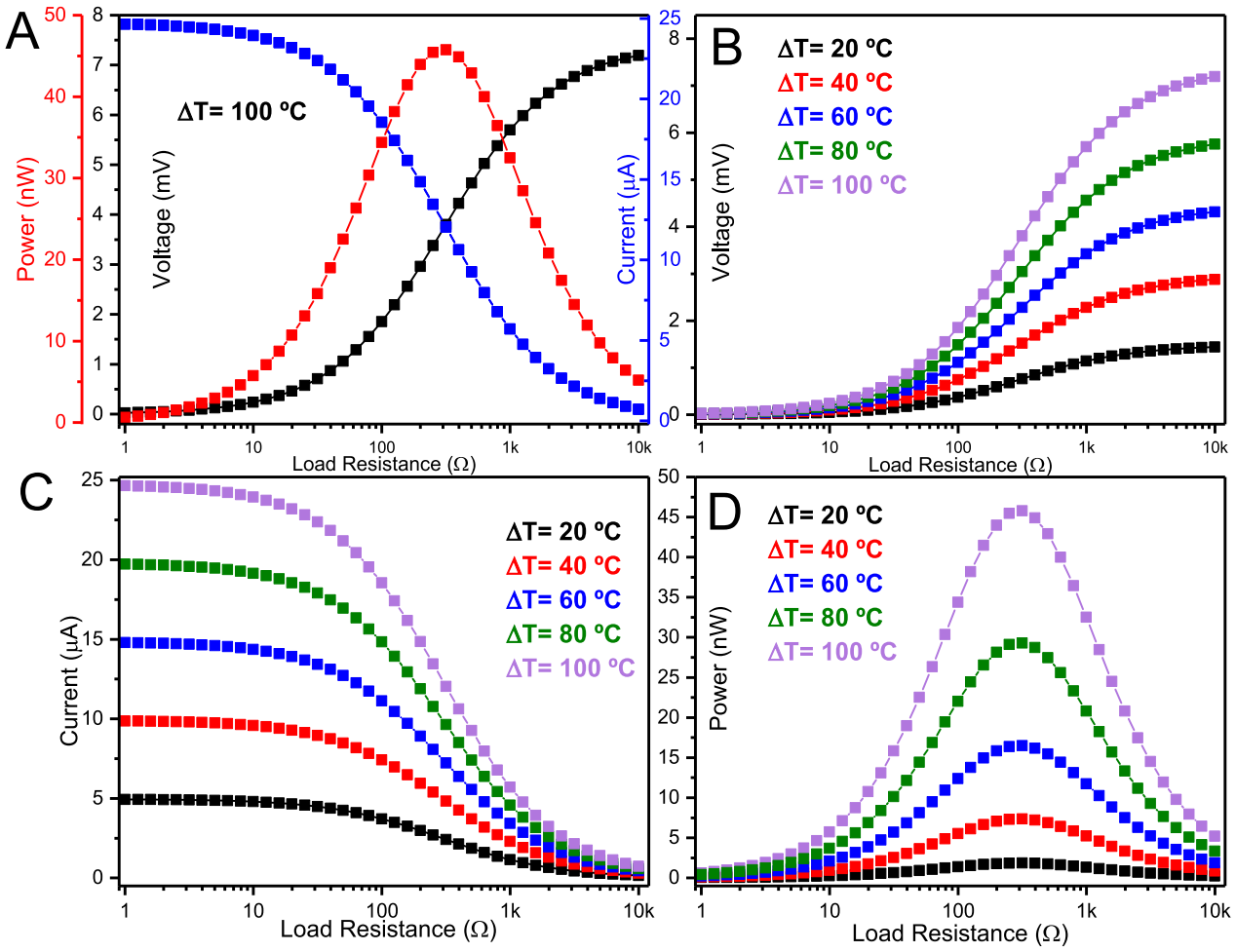

Fig. 10. Simulated thermoelectric energy harvesting performance of a single thermocouple as a function of load resistance: A) output voltage, current and power for a temperature gradient of 100 °C; B) output voltage; C) output current and D) output power for several temperature gradients.

all temperature gradients stabilizes for load resistance <1 kΩ, increasing for higher temperatures, and reaches a maximum output voltage of ≈7.5 V for ΔT = 100 °C. In the case of output current, the typical behavior is shown in Fig. 10C where the influence of temperature is similar to that of the output voltage. The maximum output power occurs at constant load resistance, independently of the temperature gradient, as represented in Fig. 10D, reaching a maximum of ≈47 nW for a ΔT = 100 °C and load resistance of ≈315 Ω.

The energy harvesting response for 2 and 4 thermocouples (Figure SI6 and SI7) is similar to the one obtained for a single thermocouple, as represented in Fig. 10. The voltage, current, and power output as a function of load resistance is shown (for 2 and 4 thermocouples) in Fig. 11A and B for ΔT = 100 °C, respectively. The output voltage and current (Fig. 11B) showed a similar influence of the temperature on the output signals. A maximum voltage of ≈27.5 V and a current of ≈22.5 μA for a ΔT = 100 °C were obtained for 4 thermocouples. In the case of output voltage, the increase of the number of thermocouples increases the output signal by nearly 3.6× when compared to 1 thermocouple, and for the output current, a slight decrease was observed reaching ≈23.3 μA. Finally, the output power was also enhanced with the increase of thermocouple being ≈47 nW for 1 thermocouple and increasing to ≈163 nW (3.5 × higher) for 4 thermocouples when ΔT = 100 °C and load resistance of ≈1.25 kΩ (Fig. 11B).

To predict the PVDF based thermoelectric energy harvesting performance, a linear fit was extrapolated for the load resistance when the maximum output power is obtained over the number of thermocouples. The maximum output power was also evaluated as a function of the number of thermocouples when ΔT = 100 °C is applied (Fig. 11C).

In both cases, a temperature gradient of 100 °C is applied, and the fitting function showed good fitting parameters (Origin 9.4 software) (Fig. 11D). It is shown that the increase in the number of thermocouples increases the maximum load resistance linearly, mainly due to the increase in the number of non-conductor materials (n- and p-type PVDF materials). For the prediction of output power, an exponential function shows a good fitting parameter (R2 = 0.999) considering that for a higher number of thermocouples, the heat losses due to the non-conductor behavior of the samples will lead to a lower increase in the output power obtained for a high number of the thermocouples.

4. Conclusions

Thermoelectric energy harvesting materials based on semicrystalline PVDF and amorphous SEBS have been selected as polymer matrix materials due to their extraordinary mechanical properties and ensure their homogeneous filler dispersion and material structures.

This study demonstrates that the TE performance of the materials critically depends on the filler type and contents. PVDF shows larger dielectric and thermal conductivity than SEBS, for pristine polymers and respective composites. Electrical conductivity increases near 9 orders of magnitude for ternary composites, and the thermal conductivity is higher for PVDF/50Bi_2Te_3 composite, 5× higher than pristine PVDF. This slightly changes with temperature, mainly for PVDF composites at temperatures larger than 100 °C, when semicrystalline PVDF shifts into a rubbery state. Seebeck coefficient increases with increasing TE filler

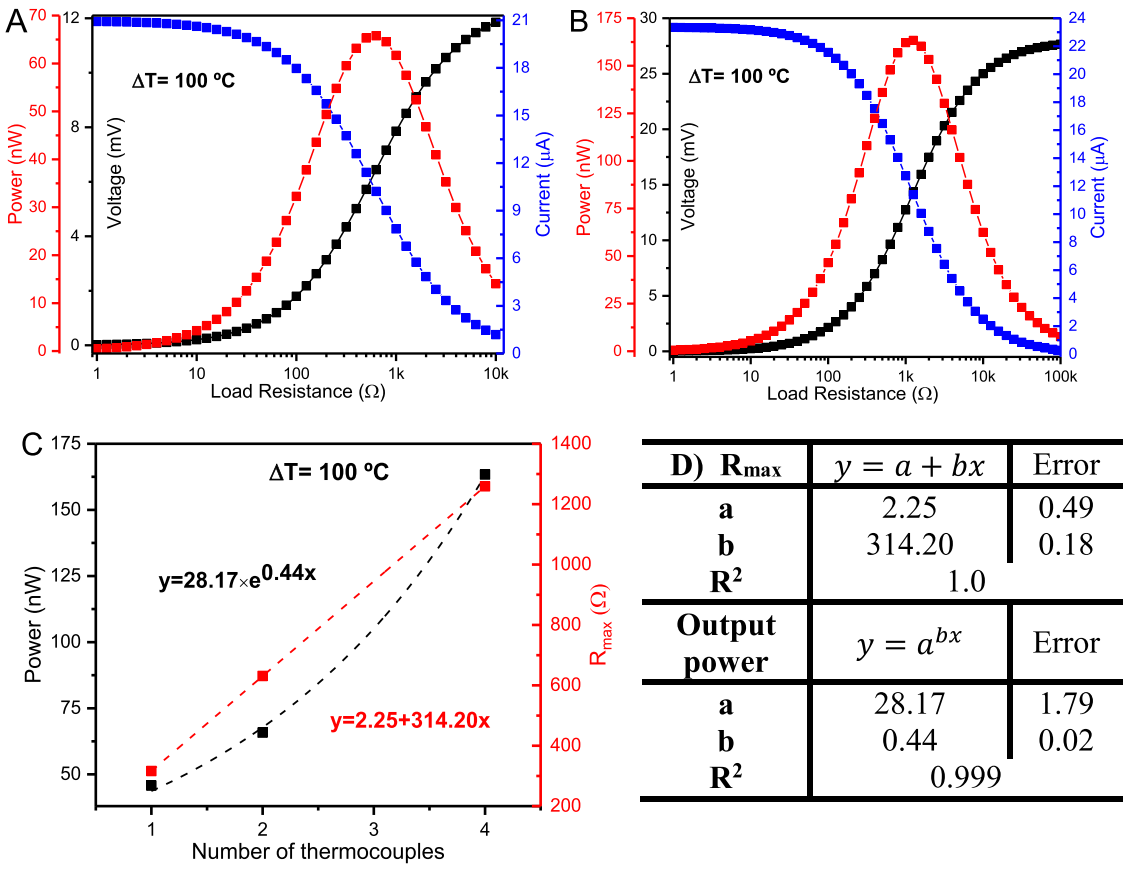

D) R_{max}	$y = a + bx$	Error
a	2.25	0.49
b	314.20	0.18
R^2	1.0	
Output power	$y = a^{bx}$	Error
a	28.17	1.79
b	0.44	0.02
R^2	0.999	

Fig. 11. Simulated thermoelectric energy harvesting performance (output voltage, current and power) of 2 (A) and 4 (B) thermocouples as a function of load resistance for a ΔT = 100 °C. C) Fitting of the output power and respective load resistance as a function of the number of thermocouples and D) their corresponding values.

content, with the PVDF/80Bi_2S_3 the material that presents the highest Seebeck performance. The Seebeck depends more on the filler type and content than the host polymer. The ZT and PF of the different materials were obtained, and the ternary composites, show an increase near 9 orders of magnitude higher than polymers, reaching $PF \sim 10^{-3}$ μW/(m·K^2). SEBS composites present TE with similar behavior to PVDF.

Finally, when a thermocouple pair using the n- and p-type materials with the best performance (PVDF/50Bi_2S_3 and PVDF/50Bi_2Te_3), for a device composed of 2 thermocouples, the $P_{out} \sim 2.7$ nW and $V_{out} \sim 5$ V for ΔT = 100 °C, similarly result when is charged a capacitor.

In the theoretical model developed, the results obtained concur with the demonstrated experimental results. The electrical energy generation depends on the temperature gradient and, in a proof-of-concept application, on the number of pairs, as well as their intrinsic performance. The extrapolated load resistance and the respective maximum output power can also be used to tailor the polymer-based thermoelectric energy harvesting as a successful power source for low-power devices.

Declaration of Competing Interest

The authors declare that they have no known competing financial interests or personal relationships that could have appeared to influence the work reported in this paper.

Data availability

Data will be made available on request.

Acknowledgments

The authors thank the Fundação para a Ciência e Tecnologia for financial support through the Strategic Funding grants UID/FIS/04650/2021 and UIDB/00319/2020, and the support under grants SFRH/BD/140242/2018 (T.R.M) and SFRH/BPD/110914/2015 (P.C.). V.Cwas supported by Junior Investigator Contract (DL57/2016). This study forms part of the Advanced Materials program and was supported by MCIN with funding from European Union NextGenerationEU (PRTR-C17.I1) and by the Basque Government under the IKUR program. Funding from the Basque Government Industry Departments under the ELKARTEK program is also acknowledged.

Appendix A. Supplementary data

Supplementary data to this article can be found online at https://doi.org/10.1016/j.cej.2023.145297.

References

[1] C. Wu, A.C. Wang, W. Ding, H. Guo, Z.L. Wang, Triboelectric nanogenerator: a foundation of the energy for the new era, Adv. Energy Mater. 9 (1) (2019) 1802906. https://doi.org/10.1002/aenm.201802906.
[2] U.S.E.I. Administration, International Energy Outlook (2021) 2021. https://www.eia.gov/outlooks/ieo/pdf/IEO2021_Narrative.pdf.
[3] T. Ahmad, D. Zhang, A critical review of comparative global historical energy consumption and future demand: the story told so far, Energy Rep. 6 (2020) 1973–1991. https://doi.org/10.1016/j.egyr.2020.07.020.
[4] R. Kothari, V.V. Tyagi, A. Pathak, Waste-to-energy: A way from renewable energy sources to sustainable development, Renew. Sustain. Energy Rev. 14 (9) (2010) 3164–3170. https://doi.org/10.1016/j.rser.2010.05.005.
[5] A.G. Rösch, L. Franke, M.M. Mallick, U. Lemmer, Optimizing printed thermoelectric generators with geometry and processibility limitations, Energ.

Conver. Manage. 279 (2023), 116776. https://doi.org/10.1016/j.enconman.2023.116776.
[6] T. Rodrigues-Marinho, N. Perinka, P. Costa, S. Lanceros-Mendez, Printable lightweight polymer-based energy harvesting systems: materials, processes, and applications, Mater. Today Sustain. 21 (2023), 100292, https://doi.org/10.1016/j.mtsust.2022.100292.
[7] M.A. Markets, Wearable Sensors Market, 2017. https://www.marketsandmarkets.com/PressReleases/wearable-sensor.asp.
[8] I.E. Agency, Key world energy statistics, 2017. https://www.iea.org/publications/freepublications/publication/KeyWorld2017.pdf.
[9] M.A. Markets, Energy Harvesting Systems Market, 2017. https://www.marketsandmarkets.com/Market-Reports/energy-harvesting-market-734.html.
[10] M. Bharti, A. Singh, S. Samanta, D.K. Aswal, Conductive polymers for thermoelectric power generation, Prog. Mater Sci. 93 (2018) 270–310, https://doi.org/10.1016/j.pmatsci.2017.09.004.
[11] X.-L. Shi, J. Zou, Z.-G. Chen, Advanced thermoelectric design: from materials and structures to devices, Chem. Rev. 120 (15) (2020) 7399–7515, https://doi.org/10.1021/acs.chemrev.0c00026.
[12] J. Shi, X. Wu, X. Geng, L. Hu, F. Liu, W. Ao, C. Zhang, Anisotropy engineering in solution-derived nanostructured Bi2Te3 thin films for high-performance flexible thermoelectric devices, Chem. Eng. J. 458 (2023), 141450. https://doi.org/10.1016/j.cej.2023.141450.
[13] B. Russ, A. Glaudell, J.J. Urban, M.L. Chabinyc, R.A. Segalman, Organic thermoelectric materials for energy harvesting and temperature control, Nat. Rev. Mater. 1 (10) (2016) 16050, https://doi.org/10.1038/natrevmats.2016.50.
[14] N. Jaziri, A. Boughamoura, J. Müller, B. Mezghani, F. Tounsi, M. Ismail, A comprehensive review of thermoelectric generators: technologies and common applications, Energy Rep. 6 (2020) 264–287, https://doi.org/10.1016/j.egyr.2019.12.011.
[15] Q. Zhang, Y. Sun, W. Xu, D. Zhu, Organic thermoelectric materials: emerging green energy materials converting heat to electricity directly and efficiently, Adv. Mater. 26 (40) (2014) 6829–6851, https://doi.org/10.1002/adma.201305371.
[16] S. Leblanc, S.K. Yee, M.L. Scullin, C. Dames, K.E. Goodson, Material and manufacturing cost considerations for thermoelectrics, Renew. Sustain. Energy Rev. 32 (2014) 313–327, https://doi.org/10.1016/j.rser.2013.12.030.
[17] V. Jangra, S. Maity, P. Vishnoi, A review on the development of conjugated polymer-based textile thermoelectric generator, J. Ind. Text. 51 (1) (2022) 181S–214S, https://doi.org/10.1177/1528083721996732.
[18] T.M. Tritt, M.A. Subramanian, Thermoelectric materials, phenomena, and applications: A bird's eye view, MRS Bull. 31 (3) (2006) 188–198, https://doi.org/10.1557/mrs2006.44.
[19] L. Jin, Y. Hao, A.K. Tareen, K. Khan, S. Wageh, O.A. Al-Hartomy, A.G. Al-Sehemi, H. Zhang, Y. Zhang, Tellurium/polymers for flexible thermoelectrics: status and challenges, J. Mater. Chem. A 11 (8) (2023) 3771–3788, https://doi.org/10.1039/D2TA09517C.
[20] L.P. Hu, T.J. Zhu, X.Q. Yue, X.H. Liu, Y.G. Wang, Z.J. Xu, X.B. Zhao, Enhanced figure of merit in antimony telluride thermoelectric materials by In–Ag co-alloying for mid-temperature power generation, Acta Mater. 85 (2015) 270–278. https://doi.org/10.1016/j.actamat.2014.11.023.
[21] Y. Bai, T. Ouyang, X. Li, Y. Yan, Z. Kong, X. Ma, Z. Li, Z. Li, X. Cai, J. Cai, H. Tan, Boosting the thermoelectric performance of n-type Bi2S3 by compositing rGO, J. Alloy. Compd. 933 (2023), 167814. https://doi.org/10.1016/j.jallcom.2022.167814.
[22] A. Kumar, S. Bano, B. Govind, A. Bhardwaj, K. Bhatt, D.K. Misra, A review on fundamentals, design and optimization to high ZT of thermoelectric materials for application to thermoelectric technology, J. Electron. Mater. 50 (11) (2021) 6037–6059, https://doi.org/10.1007/s11664-021-09153-7.
[23] J.H. We, S.J. Kim, G.S. Kim, B.J. Cho, Improvement of thermoelectric properties of screen-printed Bi2Te3 thick film by optimization of the annealing process, J. Alloy. Compd. 552 (2013) 107–110, https://doi.org/10.1016/j.jallcom.2012.10.085.
[24] S.J. Kim, J.H. We, B.J. Cho, A wearable thermoelectric generator fabricated on a glass fabric, Energ. Environ. Sci. 7 (6) (2014) 1959–1965, https://doi.org/10.1039/C4EE00242C.
[25] T. Cao, X.-L. Shi, Z.-G. Chen, Advances in the design and assembly of flexible thermoelectric device, Prog. Mater Sci. 131 (2023), 101003. https://doi.org/10.1016/j.pmatsci.2022.101003.
[26] J.-F. Brun, C. Binet, J.-F. Tahon, A. Addad, P. Tranchard, S. Barrau, Thermoelectric properties of bulk multi-walled carbon nanotube - poly(vinylidene fluoride) nanocomposites: Study of the structure/property relationships, Synth. Met. 269 (2020) 116525.
[27] Y. Lu, Y. Ding, Y. Qiu, K. Cai, Q. Yao, H. Song, L. Tong, J. He, L. Chen, Good performance and flexible PEDOT:PSS/Cu2Se nanowire thermoelectric composite films, ACS Appl. Mater. Interfaces 11 (13) (2019) 12819–12829, https://doi.org/10.1021/acsami.9b01718.
[28] S. Mondal, D. Dhak, B. Saha, Polymer and composite based thermoelectrics: Basics, scopes and issues, Vietnam J. Chem. 60 (6) (2022) 689–699. https://doi.org/10.1002/vjch.202200118.
[29] Y. Wang, G. Liu, M. Sheng, C. Yu, Y. Deng, Flexible thermopower generation over broad temperature range by PANI/nanorod hybrid-based p-n couples, J. Mater. Chem. A 7 (4) (2019) 1718–1724, https://doi.org/10.1039/c8ta11008e.
[30] P.C. Joshi, R.R. Dehoff, C.E. Duty, W.H. Peter, R.D. Ott, L.J. Love, C.A. Blue, Direct digital additive manufacturing technologies: Path towards hybrid integration, FIIW 2012 - 2012 Future of Instrumentation International Workshop Proceedings, 2012, pp. 39-42.
[31] D. Gamota, P. Brazis, K. Kalyanasundaram, J. Zhang (Eds.), Printed Organic and Molecular Electronics, Springer US, Boston, MA, 2004.
[32] S. Khan, L. Lorenzelli, R.S. Dahiya, Technologies for printing sensors and electronics over large flexible substrates: a review, IEEE Sens. J. 15 (6) (2015) 3164–3185, https://doi.org/10.1109/JSEN.2014.2375203.
[33] A.H. Espera, J.R.C. Dizon, Q. Chen, R.C. Advincula, 3D-printing and advanced manufacturing for electronics, Prog. Addit. Manuf. 4 (3) (2019) 245–267, https://doi.org/10.1007/s40964-019-00077-7.
[34] G. Liu, X. Zhang, X. Chen, Y. He, L. Cheng, M. Huo, J. Yin, F. Hao, S. Chen, P. Wang, S. Yi, L. Wan, Z. Mao, Z. Chen, X. Wang, Z. Cao, J. Lu, Additive manufacturing of structural materials, Mater. Sci. Eng. R. Rep. 145 (2021) 100596.
[35] R. Nayak, P. Shetty, S. M, A. Rao, K.M. Rao, G. K, S. Mangavati, Enhancement of power factor of screen printed polyaniline /graphite based flexible thermoelectric generator by structural modifications, J. Alloy. Compd. 922 (2022), 166298, https://doi.org/10.1016/j.jallcom.2022.166298.
[36] J. Oliveira, V. Correia, H. Castro, P. Martins, S. Lanceros-Mendez, Polymer-based smart materials by printing technologies: Improving application and integration, Addit. Manuf. 21 (2018) 269–283. https://doi.org/10.1016/j.addma.2018.03.012.
[37] A. Chen, D. Madan, P.K. Wright, J.W. Evans, Dispenser-printed planar thick-film thermoelectric energy generators, J. Micromech. Microeng. 21 (10) (2011) 8, https://doi.org/10.1088/0960-1317/21/10/104006.
[38] A.K. Menon, O. Meek, A.J. Eng, S.K. Yee, Radial thermoelectric generator fabricated from n- and p-type conducting polymers, J. Appl. Polym. Sci. 134 (3) (2017) 8, https://doi.org/10.1002/app.44060.
[39] J.H. We, S.J. Kim, B.J. Cho, Hybrid composite of screen-printed inorganic thermoelectric film and organic conducting polymer for flexible thermoelectric power generator, Energy 73 (2014) 506–512. https://doi.org/10.1016/j.energy.2014.06.047.
[40] K. Suemori, S. Hoshino, T. Kamata, Flexible and lightweight thermoelectric generators composed of carbon nanotube-polystyrene composites printed on film substrate, Appl. Phys. Lett. 103(15) (2013) 4. https://doi.org/10.1063/1.4824648.
[41] P. Martins, A.C. Lopes, S. Lanceros-Mendez, Electroactive phases of poly (vinylidene fluoride): Determination, processing and applications, Prog. Polym. Sci. 39 (4) (2014) 683–706. https://doi.org/10.1016/j.progpolymsci.2013.07.006.
[42] J.R. Dios, C. Garcia-Astrain, S. Gonçalves, P. Costa, S. Lanceros-Méndez, Piezoresistive performance of polymer-based materials as a function of the matrix and nanofiller content to walking detection application, Compos. Sci. Technol. 181 (2019), 107678. https://doi.org/10.1016/j.compscitech.2019.107678.
[43] Y. Wang, M. Yao, R. Ma, Q. Yuan, D. Yang, B. Cui, C. Ma, M. Liu, D. Hu, Design strategy of barium titanate/polyvinylidene fluoride-based nanocomposite films for high energy storage, J. Mater. Chem. A 8 (3) (2020) 884–917, https://doi.org/10.1039/C9TA11527G.
[44] N. Sezer, M. Koç, A comprehensive review on the state-of-the-art of piezoelectric energy harvesting, Nano Energy 80 (2021), 105567. https://doi.org/10.1016/j.nanoen.2020.105567.
[45] I. Paulraj, V. Lourdhusamy, C.-J. Liu, Organic/Inorganic n-type PVDF/Cu0.6Ni0.4 hybrid composites for thermoelectric application: a thermoelectric generator made of 8 pairs of p-leg ZnSb/Sb and n-leg β-PVDF/Cu0.6Ni0.4, Chem. Eng. J. 446 (2022), 137083. https://doi.org/10.1016/j.cej.2022.137083.
[46] P. Costa, A. Maceiras, M. San Sebastián, C. García-Astrain, J.L. Vilas, S. Lanceros-Mendez, On the use of surfactants for improving nanofiller dispersion and piezoresistive response in stretchable polymer composites, J. Mater. Chem. C 6 (39) (2018) 10580–10588.
[47] T.H. Kwan, Y.C. Zhang, Q.H. Yao, A coupled 3D electrochemical and thermal numerical analysis of the hybrid fuel cell-thermoelectric device system, Int. J. Hydrogen Energy 43 (52) (2018) 23450–23462, https://doi.org/10.1016/j.ijhydene.2018.10.202.
[48] L. Francioso, C. De Pascali, P. Siciliano, Experimental assessment of thermoelectric generator package properties: Simulated results validation and real gradient capabilities, Energy 86 (2015) 300–310, https://doi.org/10.1016/j.energy.2015.04.041.
[49] L. Youhong, Z. Yingzeng, X. Qingpei, H. Fanhua, A. Qi, C. Haodong, Comprehensive modeling and parametric analysis of multi-mission thermoelectric generator, Appl. Therm. Eng. 219 (2023), https://doi.org/10.1016/j.applthermaleng.2022.119447.
[50] Y. Bormashenko, R. Pogreb, O. Stanevsky, E. Bormashenko, Vibrational spectrum of PVDF and its interpretation, Polym. Test. 23 (7) (2004) 791–796. https://doi.org/10.1016/j.polymertesting.2004.04.001.
[51] V. Elumalai, R. Annapooranan, M. Ganapathikrishnan, D. Sangeetha, A synthesis study of phosphonated PSEBS for high temperature proton exchange membrane fuel cells, J. Appl. Polym. Sci. 135 (10) (2018) 45954.
[52] P. Costa, J. Silva, A. Ansón-Casaos, M.T. Martinez, M.J. Abad, J. Viana, S. Lanceros-Mendez, Effect of carbon nanotube type and functionalization on the electrical, thermal, mechanical and electromechanical properties of carbon nanotube/styrene–butadiene–styrene composites for large strain sensor applications, Compos. B Eng. 61 (2014) 136–146. https://doi.org/10.1016/j.compositesb.2014.01.048.
[53] P. Costa, C. Silvia, J.C. Viana, S. Lanceros Mendez, Extruded thermoplastic elastomers styrene–butadiene–styrene/carbon nanotubes composites for strain sensor applications, Compos. B Eng. 57 (2014) 242–249. https://doi.org/10.1016/j.compositesb.2013.10.006.
[54] Y. Shi, Z. Zhao, W. Liu, C. Zhang, Physically Self-Cross-Linked SEBS anion exchange membranes, Energy Fuel 34 (12) (2020) 16746–16755, https://doi.org/10.1021/acs.energyfuels.0c03017.
[55] D.P. Jena, B. Mohanty, R.K. Parida, B.N. Parida, N.C. Nayak, Dielectric and thermal behavior of 0.75BiFeO3-0.25BaTiO3 filled ethylene vinyl acetate composites, Mater. Chem. Phys. 243 (2020), 122527, https://doi.org/10.1016/j.matchemphys.2019.122527.

[56] M. Yaprintsev, A. Vasil'ev, O. Ivanov, M. Zhezhu, E. Yaprintseva, V. Novikov, Enhanced thermoelectric efficiency of the bulk composites consisting of "Bi2Te3 matrix" and "filler Ni@NiTe2 inclusions", Scr. Mater. 194 (2021), 113710. https://doi.org/10.1016/j.scriptamat.2020.113710.
[57] J.A. Puértolas, J.F. García-García, F.J. Pascual, J.M. González-Domínguez, M. T. Martínez, A. Ansón-Casaos, Dielectric behavior and electrical conductivity of PVDF filled with functionalized single-walled carbon nanotubes, Compos. Sci. Technol. 152 (2017) 263–274. https://doi.org/10.1016/j.compscitech.2017.09.016.
[58] A.M. Gaur, D.S. Rana, In situ measurement of dielectric permittivity and electrical conductivity of CoCl2/BaCl2 Doped PVDF composite at elevated temperature, J. Inorg. Organomet. Polym Mater. 29 (5) (2019) 1637–1644, https://doi.org/10.1007/s10904-019-01126-y.
[59] X. Xia, G.J. Weng, J. Zhang, Y. Li, The effect of temperature and graphene concentration on the electrical conductivity and dielectric permittivity of graphene–polymer nanocomposites, Acta Mech. 231 (4) (2020) 1305–1320, https://doi.org/10.1007/s00707-019-02588-4.
[60] M. Mohiuddin, S.V. Hoa, Temperature dependent electrical conductivity of CNT–PEEK composites, Compos. Sci. Technol. 72 (1) (2011) 21–27. https://doi.org/10.1016/j.compscitech.2011.08.018.
[61] G. Prunet, F. Pawula, G. Fleury, E. Cloutet, A.J. Robinson, G. Hadziioannou, A. Pakdel, A review on conductive polymers and their hybrids for flexible and wearable thermoelectric applications, Mat. Today Phy. 18 (2021) 100402.
[62] P. Costa, J. Silva, S. Lanceros Mendez, Strong increase of the dielectric response of carbon nanotube/poly(vinylidene fluoride) composites induced by carbon nanotube type and pre-treatment, Compos. B Eng. 93 (2016) 310–316. https://doi.org/10.1016/j.compositesb.2016.03.010.
[63] S. Tu, Q. Jiang, X. Zhang, H.N. Alshareef, Large dielectric constant enhancement in MXene percolative polymer composites, ACS Nano 12 (4) (2018) 3369–3377, https://doi.org/10.1021/acsnano.7b08895.
[64] T. Marinho, P. Costa, E. Lizundia, C.M. Costa, S. Corona-Galván, S. Lanceros-Méndez, Ceramic nanoparticles and carbon nanotubes reinforced thermoplastic materials for piezocapacitive sensing applications, Compos. Sci. Technol. 183 (2019), 107804. https://doi.org/10.1016/j.compscitech.2019.107804.
[65] R. Li, X. Yang, J. Li, Y. Shen, L. Zhang, R. Lu, C. Wang, X. Zheng, H. Chen, T. Zhang, Review on polymer composites with high thermal conductivity and low dielectric properties for electronic packaging, Mat. Today Phy. 22 (2022), 100594. https://doi.org/10.1016/j.mtphys.2021.100594.
[66] R. Ram, V. Soni, D. Khastgir, Electrical and thermal conductivity of polyvinylidene fluoride (PVDF) – Conducting Carbon Black (CCB) composites: validation of various theoretical models, Compos. B Eng. 185 (2020), 107748. https://doi.org/10.1016/j.compositesb.2020.107748.
[67] A. Kumar, R. Kumar, D.K. Satapathy, Bi2Se3-PVDF composite: A flexible thermoelectric system, Phys. B Condens. Matter 593 (2020), 412275. https://doi.org/10.1016/j.physb.2020.412275.
[68] Y. Guo, K. Ruan, X. Shi, X. Yang, J. Gu, Factors affecting thermal conductivities of the polymers and polymer composites: a review, Compos. Sci. Technol. 193 (2020), 108134. https://doi.org/10.1016/j.compscitech.2020.108134.
[69] Y.S. Hor, A.J. Williams, J.G. Checkelsky, P. Roushan, J. Seo, Q. Xu, H. W. Zandbergen, A. Yazdani, N.P. Ong, R.J. Cava, Superconductivity in ${\mathrm{Cu}}_{x}{\mathrm{Bi}}_{2}{\mathrm{Se}}_{3}$ and its implications for pairing in the undoped topological insulator, Phys. Rev. Lett. 104 (5) (2010), 057001, https://doi.org/10.1103/PhysRevLett.104.057001.
[70] A. Chen, D. Madan, P.K. Wright, J.W. Evans, Dispenser-printed planar thick-film thermoelectric energy generators, J. Micromech. Microeng. 21 (10) (2011), 104006, https://doi.org/10.1088/0960-1317/21/10/104006.
[71] Y. Zhang, K.Y. Rhee, S.-J. Park, Facile design of a domestic thermoelectric generator by tailoring the thermoelectric performance of volume-controlled expanded graphite/PVDF composites, Compos. B Eng. 176 (2019), 107234. https://doi.org/10.1016/j.compositesb.2019.107234.
[72] S. Hu, S. Zeng, X. Li, J. Jiang, W. Yang, Y. Chen, M. Li, J. Zheng, Flexible and high performance of n-type thermoelectric PVDF composite film induced by nickel nanowires, Mater. Des. 188 (2020), 108496, https://doi.org/10.1016/j.matdes.2020.108496.
[73] Y.-C. Sun, D. Terakita, A.C. Tseng, H.E. Naguib, Study on the thermoelectric properties of PVDF/MWCNT and PVDF/GNP composite foam, Smart Mater. Struct. 24 (8) (2015), 085034, https://doi.org/10.1088/0964-1726/24/8/085034.
[74] Z. Liang, H.H. Choi, X. Luo, T. Liu, A. Abtahi, U.S. Ramasamy, J.A. Hitron, K. N. Baustert, J.L. Hempel, A.M. Boehm, A. Ansary, D.R. Strachan, J. Mei, C. Risko, V. Podzorov, K.R. Graham, n-type charge transport in heavily p-doped polymers, Nat. Mater. 20 (4) (2021) 518–524, https://doi.org/10.1038/s41563-020-00859-3.
[75] M.S. Hossain, T. Li, Y. Yu, J. Yong, J.H. Bahk, E. Skafidas, Recent advances in printable thermoelectric devices: materials, printing techniques, and applications, RSC Adv. 10 (14) (2020) 8421–8434, https://doi.org/10.1039/c9ra09801a.
[76] N. Nandihalli, C.-J. Liu, T. Mori, Polymer based thermoelectric nanocomposite materials and devices: fabrication and characteristics, Nano Energy 78 (2020), 105186. https://doi.org/10.1016/j.nanoen.2020.105186.
[77] C. Dun, C.A. Hewitt, H. Huang, J. Xu, D.S. Montgomery, W. Nie, Q. Jiang, D. L. Carroll, Layered Bi2Se3 nanoplate/polyvinylidene fluoride composite based n-type thermoelectric fabrics, ACS Appl. Mater. Interfaces 7 (13) (2015) 7054–7059, https://doi.org/10.1021/acsami.5b00514.
[78] A. Dadhich, M. Saminathan, K. Kumari, S. Perumal, M.S. Ramachandra Rao, K. Sethupathi, Physics and technology of thermoelectric materials and devices, J. Phys. D Appl. Phys. 56 (33) (2023), 333001, https://doi.org/10.1088/1361-6463/acc9d0.
[79] Y. Pei, H. Wang, G.J. Snyder, Band engineering of thermoelectric materials, Adv. Mater. 24 (46) (2012) 6125–6135. https://doi.org/10.1002/adma.201202919.
[80] S. Sharma, H.H. Singh, S. Kumar, N. Khare, PANI coupled hierarchical Bi2S3 nanoflowers based hybrid nanocomposite for enhanced thermoelectric performance, Nanotechnology 32 (33) (2021), 335705, https://doi.org/10.1088/1361-6528/abeeb7.
[81] Y. Na, S. Kim, S.P.R. Mallem, S. Yi, K.T. Kim, K.-I. Park, Energy harvesting from human body heat using highly flexible thermoelectric generator based on Bi2Te3 particles and polymer composite, J. Alloy. Compd. 924 (2022), 166575. https://doi.org/10.1016/j.jallcom.2022.166575.
[82] S. Kumar, H.H. Singh, N. Khare, Flexible hybrid piezoelectric-thermoelectric generator for harnessing electrical energy from mechanical and thermal energy, Energ. Conver. Manage. 198 (2019), 111783. https://doi.org/10.1016/j.enconman.2019.111783.
[83] H. Cheng, X. He, Z. Fan, J. Ouyang, Flexible quasi-solid state ionogels with remarkable seebeck coefficient and high thermoelectric properties, Adv. Energy Mater. 9 (32) (2019), 1901085. https://doi.org/10.1002/aenm.201901085.
[84] C. Dun, C.A. Hewitt, H. Huang, J. Xu, C. Zhou, W. Huang, Y. Cui, W. Zhou, Q. Jiang, D.L. Carroll, Flexible n-type thermoelectric films based on Cu-doped Bi2Se3 nanoplate and Polyvinylidene Fluoride composite with decoupled Seebeck coefficient and electrical conductivity, Nano Energy 18 (2015) 306–314. https://doi.org/10.1016/j.nanoen.2015.10.012.
[85] H. Zhou, Z. Zhang, C. Sun, H. Deng, Q. Fu, Biomimetic approach to facilitate the high filler content in free-standing and flexible thermoelectric polymer composite films based on PVDF and Ag2Se nanowires, ACS Appl. Mater. Interfaces 12 (46) (2020) 51506–51516, https://doi.org/10.1021/acsami.0c15414.
[86] H. Zhou, Y. Zhang, Y. Qiu, H. Wu, W. Qin, Y. Liao, Q. Yu, H. Cheng, Stretchable piezoelectric energy harvesters and self-powered sensors for wearable and implantable devices, Biosens. Bioelectron. 168 (2020), 112569. https://doi.org/10.1016/j.bios.2020.112569.
[87] Y. Zhang, R. Lu, S. Zhang, B. Tang, Intelligent light-driven flexible solar thermoelectric system, Chem. Eng. J. 423 (2021), 130260, https://doi.org/10.1016/j.cej.2021.130260.
[88] B. Krause, C. Barbier, J. Levente, M. Klaus, P. Pötschke, Screening of different carbon nanotubes in melt-mixed polymer composites with different polymer matrices for their thermoelectrical properties, J. Compos. Sci. 3 (4) (2019) 106.
[89] C. Navone, M. Soulier, M. Plissonnier, A.L. Seiler, Development of (Bi,Sb)2(Te,Se)3-based thermoelectric modules by a screen-printing process, J. Electron. Mater. 39 (9) (2010) 1755–1759, https://doi.org/10.1007/s11664-010-1187-3.
[90] Y. Wang, L. Yang, X.L. Shi, X. Shi, L. Chen, M.S. Dargusch, J. Zou, Z.G. Chen, Flexible thermoelectric materials and generators: challenges and innovations, Adv. Mater. 31 (29) (2019), https://doi.org/10.1002/adma.201807916.